Crystal-tolerant glass approach for mitigation of crystal accumulation in continuous melters processing radioactive waste

Josef Matyáš,[*,†] Adam R Huckleberry,[†] Carmen P Rodriguez,[†] Jesse B Lang,[†] Antoinette T Owen,[†] and Albert A Kruger[‡]

[†]*Pacific Northwest National Laboratory; PO Box 999; Richland, WA, USA 99352*

[‡]*Office of River Protection, P.O. Box 450; Richland, WA, USA 99352*

Keywords: High-level waste; Vitrification; Melter; Spinel crystals; Accumulation; Empirical model; Agglomeration; Liquidus temperature; Crystal-tolerant glass

Abstract

High-level radioactive waste melters are projected to operate in an inefficient manner as they are subjected to artificial constraints, such as minimum liquidus temperature (T_L) or maximum equilibrium fraction of crystallinity at a given temperature. These constraints substantially limit waste loading, but were imposed to prevent clogging of the melter with spinel crystals [(Fe, Ni, Mn, Zn)(Fe, Cr)$_2$O$_4$]. In the melter, the glass discharge riser is the most likely location for crystal accumulation during idling because of low glass temperatures, stagnant melts, and small diameter. To address this problem, a series of lab-scale crucible tests were performed with specially formulated glasses to simulate accumulation of spinel in the riser. Thicknesses of accumulated layers were incorporated into empirical model of spinel settling. In addition, T_L of glasses was measured and impact of particle agglomeration on accumulation rate was evaluated. Empirical model predicted well the accumulation of single crystals and/or small-scale agglomerates, but, excessive agglomeration observed in high-Ni-Fe glass resulted in an

---

[*] Corresponding author: Josef.Matyas@pnnl.gov; phone: 1 (509) 372-6023; fax 1 (509) 372-5997

under-prediction of accumulated layers, which gradually worsen over time as an increased number of agglomerates formed. Accumulation rate of ~14.9 ± 1 nm/s determined for this glass will result in ~26 mm thick layer in 20 days of melter idling.

1. Introduction

The Joule-heated ceramic melter is technology of the choice for vitrification of high-level radioactive waste (HLW) from the Hanford and Savannah River Sites in stable borosilicate glass for long-term storage and disposal. However, current melters (Figure **1**) are periodically idled and are projected to operate in an inefficient manner as they are subjected to artificial constraints that limit waste loading to far below its intrinsic level.[1] These constraints, such as liquidus temperature (T_L) of glass or the temperature at which the equilibrium fraction of spinel crystals in the melt is below 1 vol% ($T_{0.01}$), nominally below 1050 °C, were imposed to prevent clogging of the melter with spinel crystals that can accumulate at the bottom and in the 76-mm-diameter glass discharge riser based upon operational experience with static melters (i.e., unstirred either mechanically or bubbling).[2]

Matyáš et al.[3] showed through mathematical modeling that T_L has little impact on the rate of settling and, in contrast, the crystal size is the main rate-limiting factor in crystal accumulation. Therefore, while being conservative and costly, the constraints cannot prevent the formation, growth, and accumulation of spinel crystals in considerably cooler regions (~850 °C) of the glass discharge riser during melter idling. At this temperature, a significant volume of large octahedral spinel crystals [(Fe, Ni, Mn, Zn)(Fe, Cr)$_2$O$_4$] can precipitate in the glass.[4] Matyáš et al.[5] demonstrated that these crystals (Figure 2 and Figure 3) rapidly settle, forming a thick sludge layer at rates up to 0.6 mm/d. This settling rate is fast enough to form >10 mm-thick layer that can partially or completely block the riser during melter idle, thereby preventing molten glass from discharging during normal operation. This is aggravated by the fact that the spinel sludge cannot be dissolved at low temperatures in the riser and cannot be easily disturbed.[6,7]

To minimize the accumulation of spinel crystals, attention has been focused on the behavior of spinel crystals in HLW borosilicate glasses, such as the equilibrium fraction of spinel, spinel crystallization kinetics, spinel settling rate, and the rheology of spinel sludge. Stachnik et al.[8] investigated the equilibrium mass fraction of spinel as a function of the Fe, Ni, and Cr oxides, indicating that Ni-rich glass precipitated more than three times higher concentration of spinel compared to Fe and Cr-rich glasses. Wilson et al.[9] went further by determining the equilibrium mass fraction as a function of temperature and concentration of Al, Cr, Fe, Li, Mg, Na, and Ni oxides. This study[9] confirmed a significant increase in concentration of spinel crystals in Ni-rich glasses and indicated that this increase is augmented by Fe, Al, and Mg and mitigated by Na and Li. Later, Jiricka et al.[10] studied spinel phase equilibria in low-silica HLW glasses and showed that Ni and Cr increased T_L most , but Cr affected the T_L much less in glasses with high-SiO_2 glasses.

Alton et al.[11] focused on experimental measurements of spinel crystallization in 11-component generic HLW glass (MS-7) with T_L = 1078 °C and determined the mass transfer coefficients for dissolution and growth in Hixson-Crowell equation. Izak et al.[4] investigated the effect of minor components on spinel crystallization during feed-to-glass conversion for the same glass and stated that, while Ag_2O and CuO did not help nucleate spinel, the RuO_2 increased the crystal number density (n_s) by two orders of magnitude and significantly decreased the crystal size. They also indicated that some submicrometer spinel from cold-cap (feed pile) can be passed into the melt and provide nucleation sites for crystallization of spinel in the molten glass.

Alton et al.[12] followed with a statement that the noble metals (Rh, Ru, Pd, and Pt) increased n_s independently of temperature by up to four orders of magnitude compared with MS-7 baseline glass.

The settling of spinel crystals in molten glasses[5,13-15] as well as transparent liquids[16,17] have been studied. Lamont and Hrma[13] observed the parabolic shape of the settling front indicating that the settling crystals generated a convective cell within the melt. Kloužek et al.[14] measured the settling distances between the glass level and the uppermost crystals in the centerline of the crucible and determined they were less than 10% smaller than the distances calculated with the modified Stoke's law. Matyáš et al.[5] determined the accumulation rate of crystals as a function of spinel-forming components and noble metals, and revealed a beneficial effect of suppressing the crystal size and accumulation rate through additions of Fe and noble metals. Matlack et al.[15] reported that glasses containing up to 4.2 vol% crystals have been successfully discharged from the DuraMelter® DM-100 after 8 d of melter idling at 950 °C.

To improve accumulation rate predictions, Matyáš et al.[17] studied the settling of particles in silicone oils with a developed optical particle-dynamics-analyzer, and determined the shape factors for individual spinel crystals and agglomerates. Recently, Matyáš et al.[16] determined that the Stokes and Richardson-Zaki equations can be applied to adequately predict the accumulation rate for different concentrations of spinel crystals in the glass discharge riser of HLW melter.

Our long-term objective is to develop an empirical model that can be used to calculate the crystal accumulation in the riser as a function of glass composition, providing the guidance to formulate crystal-tolerant glasses for higher waste loading.[5] By keeping the spinel crystals small and therefore limiting spinel deposition in the melter, high waste-containing glasses can be produced without decreasing melter lifetime. The thicknesses of accumulated layers as a function of the concentration of spinel-forming components can be calculated with the empirical model with good agreement with observed thicknesses.[16]

In the study reported here, a series of lab-scale crucible tests were performed on specifically formulated glasses to investigate and simulate the effect of Cr, Ni, Fe, Al, Li, and Ru oxides on the accumulation rate of spinel crystals in the glass discharge riser. The thicknesses of accumulated layers were incorporated into a previously-developed empirical model of spinel settling. We also investigated the impact of agglomerates on the accumulation rate and measured T_L as a function of temperature and composition.

2. Materials

2.1 AZ-101 Simulant

In the study, AZ-101 simulant was used as a substitute for the actual radioactive waste from Hanford Tank 241-AZ-101. A total of 85 kg of non-radioactive dry-powder of this simulant was supplied by Noah Technologies Corp. The simulant which was derived from a combination of actual AZ-101 sludge with a portion of cesium ion exchange concentrate[18] did not contain noble metals and its particle size ranged from 50 to 200 µm. Table 1 shows the composition of the simulant in mass fraction of oxides and halogens that will remain in the glass.

A representative sample of simulant was analyzed by Southwest Research Institute (SWRI) to check an agreement with the target composition from literature[18]. Methods blanks, spikes, and reference glass standards (National Institute for Standards and Technology [NIST] SRM 278 Obsidian Rock and NIST SRM 688 Basalt Rock) were used to assess the analytical precision and accuracy of inductively-coupled plasma-mass spectrometry (ICP-MS) and inductively coupled plasma-atomic emission spectroscopy (ICP-AES). The simulant was dissolved for analysis with four techniques: 1) $LiBO_2/Li_2B_4O_7$ fusion to determine Al, Ba, Ca, Cr, Co, Fe, Mn, P, Si, Na, Sn, Ti, and Zr; 2) HF/HNO_3 digestion to determine Ru; 3) $HNO_3/HCl/HF$ digestion in closed vessel to determine B and S; and 4) $HNO_3/HClO_4/HF/HCl$ digestion in open vessel to determine Cd, Cu, La, Pb, Li, Mg, Mo, Ni, K, Rh, and Zn. Produced solutions were analyzed for Co, Rh, Ru, Ti, and Zn with ICP-MS and for all other metals with ICP-AES.

Table 2 compares analyzed composition of the simulant with the composition data from Eibling et al.[18]. The concentrations of the components were within the specified criteria (based on the levels of accuracy that were accepted in the simulant as originally prepared at the Savannah River National Laboratory). The large relative percent differences (RPD) for some components illustrate the impact of analytical errors and systematic small-scale errors introduced during the simulant preparation.

2.2 HLW Glasses

Table 3 shows the target composition of glasses designed to study accumulation of spinel crystals. A composition of baseline glass from previous investigations[5,16] was varied one or two components-at-a-time while proportionally decreasing the concentration of all other components.

Eight glasses were prepared from AZ-101 simulant and additives (H_3BO_3, SiO_2, and carbonates of Li and Na). Additional Ni, Al, Cr, Fe, Li, and Rh oxides were added. Trace quantities of Ru as ruthenium nitrosyl nitrate solution, $Ru(NO)(NO_3)_x(OH)_y$, were added drop by drop to SiO_2 that was dispersed on a Petri dish. The SiO_2 cake was dried at 105 °C for 1 h, quenched, and hand-mixed in the plastic bag with the rest of the batch. The combined batch for

500 g of glass was then homogenized in an agate mill for 5 min, melted in Pt/10%Rh crucible in air at 1200 °C for an hour, air quenched, and ground in a tungsten carbide mill for 2 min. The glass powder was then remelted under the same conditions, air-quenched, and a small fraction of glass used to prepare glass chips for T_L testing. The remaining larger fraction of glass was ground in a tungsten carbide mill for 2 min and used for crystal accumulation testing. Six glass batches were prepared for each glass composition.

Table 4 shows the glass compositions used to study particle agglomeration. A baseline and high-Ni glasses from previous investigations[5,16] were altered one-at-a-time to accommodate 0.29 mass% of RuO_2. These glasses were prepared following the same procedure as described above. Trace quantities of elemental Ru were added in the form of ruthenium nitrosyl nitrate solution, Rh as Rh_2O_3, and additional Ni for high-Ni glass as NiO. The batch size was ~150 g of glass. This mass filled the test assembly and allowed us to keep the concentration of noble metal particles in the glass about the same in every assembly. Eight glass batches were prepared for each glass composition.

3. Experimental Procedures and Methods

3.1 Liquidus Temperature

The liquidus temperatures were obtained through heat-treatments at selected temperatures for 24 h in Pt/10%Rh boxes with tight fitting lids in accordance with ASTM C 1720-11[19]. Two glass samples were produced at each temperature. First sample was analyzed with a high-magnification optical microscope for the presence of crystals and the second with an XRD for the spinel content. The liquidus temperature was determined within 6 °C of the temperature range between the highest and the lowest temperature at which a sample did or did not contain spinel crystals in the glass, respectively.

3.2 Crystal Accumulation Testing

Figure 4 shows the cross-section of the double-crucible assembly. In this assembly, the alumina crucible was nested in a larger silica crucible so that molten glass covered the alumina crucible and eliminated Marangoni convection in the meniscus and bubble generation at the bottom of silica crucibles (undisturbed settling).[5,16] The core-drilled second silica crucible held the alumina crucible in place and filled the remaining space, saving more than 0.5 kg of glass per test. To minimize the effect of the surface crystallization and to eliminate the impact of thermal history on crystal nucleation and growth, powdered glass was melted in a Pt-crucible at 1200 °C for 1 h. The crucible was removed from the melting furnace and molten glass poured into three double crucibles that were rested inside the furnace at 850 °C, mimicking the temperature in the discharge riser of an actual glass melter. Double-crucibles were removed at various times, air-quenched, and cross-sectioned. Thin-sections of the bottom were prepared and analyzed with optical microscopy, SEM-EDS, and Clemex Vision PE 6.0 (Clemex Technologies Inc., Quebec, Canada) image analysis software to determine the thickness of the spinel sludge layer, shape, size, and surface fraction of spinel crystals in the accumulated layers.

3.3 Particle Agglomeration Testing

Figure 5 shows the testing assembly that was used in the lab-scale study of the particle agglomeration. The assembly consisted of an alumina crucible with an outer and inner diameter of 18 and 15 mm, respectively, and height 90 mm that was positioned on the alumina plate inside a Pt-crucible with a diameter of 30 mm and height 100 mm. The fabricated glasses were first melted in Pt/10%Rh crucibles at 1200 °C for an hour, and then the crucibles were removed one by one from the melting furnace, and molten glass poured into each of four assemblies that were rested on the 0.5-m-diameter platform inside the Deltech furnace (Deltech Inc., Denver, CO, USA) at 850 °C. These assemblies were covered with a lid and removed (air-quenched) at different times up to 4 d. The alumina crucibles were core-drilled from assemblies and investigated with X-ray tomography for the size and distribution of agglomerates. Then, the thin sections were prepared for SEM-EDS observations, and an image analysis.

3.4 X-Ray Microfocus Computed Tomography

North Star Imaging (NSI) X-View Digital X-ray Imaging and Microfocus Computed Tomography (CT) system (NSI Inc., Rogers, MN, USA) was used to study particle agglomeration. The core-drilled alumina crucibles were scanned at 110 kV and 354 mA. Total of 1441 projections were taken over 360°. Total scanning time was about 3 h. For both energies, a beam-hardening filter (1.25 mm steel) was used in order to reduce or eliminate streak artifacts. The reconstruction used was a filtered back projection, which resulted in images of 1506 x 1890 pixels. The samples were analyzed with a resolution of 17.5 µm (the smallest agglomerate that can be detected). The image analysis focused on the area ~30×15 mm inside the crucible at the bottom which was covered by 1714 XY (top view) and 857 XZ (side view) slices.

3.5 X-ray Diffraction

Glass samples were ground for 2 min in a tungsten carbide mill. Approximately 1 g of sample powder was mixed with 5 mass% of internal standard (CaF_2) for 1 min in a tungsten carbide mill, mounted in an X-ray diffraction (XRD) sample holder, and scanned with an X-ray diffractometer Bruker D8 Advanced (Bruker AXS Inc., Madison, WI, USA) configured with a Cu Kα target ($\lambda = 1.5406$ Å) set to a power level of 40 kV and 40 mA, goniometer radius of 250 mm, 0.3° fixed divergence slit, and position-sensitive detector LynxEyeTM with an angular range of 3° 2θ. The scan parameters were 0.03° 2 θ step size, 4 s dwell time, and 5 to 70° 2-θ scan range. The detection limit of XRD for spinel was 0.1 mass%. Jade 6.0 software (Materials Data Inc, Livermore, CA, USA) equipped with both the International Center of Crystallographic Data (ICCD) powder diffraction file 2 (PDF2) release 1999 and the International Center of Structure Data (ICSD) release 2004 was used to identify crystalline phases, and RIQAS 3.1 software (Materials Data Inc, Livermore, CA, USA) to determine their quantitative fractions.

3.6 Scanning Electron Microscopy and Energy Dispersive Spectroscopy

Scanning electron microscopy was used to investigate the morphology of crystals and agglomerates. Thin sections of selected glass samples were sputter-coated with Au/Pd and analyzed with a JEOL JSM-5900 from (JEOL Ltd., Tokyo, Japan) equipped with EDAX Li-drifted Si detector cooled with liquid nitrogen (Ametek Inc., Berwyn, PA, USA).

4. Results and Discussion

4.1 Liquidus Temperature

The XRD mass fraction of spinel (C_0) at different temperatures is shown in Figure 6. If we assume that the fraction of spinel at $T \geq 850$ °C and $t \geq 24$ h no longer changes with time, we can use Eq. (1) to fit the XRD data:

$$C_0 = C_{\max}\left\{1 - \exp\left[-B_L\left(\frac{1}{T} - \frac{1}{T_L}\right)\right]\right\} \qquad (1)$$

where B_L (K) and C_{max} (mass fraction) are composition-dependent coefficients, T is the temperature as measured with thermocouple (K), and T_L is the liquidus temperature (K); C_{max} can be interpreted as the hypothetical total (crystalline and dissolved) spinel in glass and B_L represents the rate of change of C_0 at $T = T_L$. Table 5 shows the calculated values for the parameters in Eq. (1) from a least squares fit of the data and the liquidus temperatures as determined with optical microscopy for different glasses. The calculated values for T_L agreed well with those measured. The small discrepancy in T_L values can be explained from the uncertainty in the XRD data. The T_L (as determined with optical microscopy) for previously measured Ni1.5 glass was 1080 °C.[5,16] Adding Li_2O, Cr_2O_3, or Al_2O_3 individually to this glass decreased T_L to 1004 °C, 1018 °C, and 1075 °C, respectively. In contrast, adding 0.015 mass% of RuO_2 or 3.12 mass % of Fe_2O_3 increased the T_L to 1087 °C and 1105 °C, respectively. Not surprisingly, introduction of more RuO_2 (0.087 mass%) to Ni1.5 glass did not change the T_L (1085 °C).

Table 6 summarizes mass and volume concentrations of spinel crystals in the glasses heat-treated at 850 °C for 24 h. More than 3 mass% (> 1.5 vol%) of crystals formed in all the glasses except for Cr0.3 (0.9 mass%) and Ni1.29 (2.7 mass%). The high concentration of spinel, 5.3 mass%, in the Ni1.5/Fe17.5 glass is the result of adding additional Fe_2O_3 to these glasses for spinel nucleation and growth.

4.2 Morphology and Size of Accumulated Crystals with Optical Microscopy

Figure 7, Figure **8**, and Figure **9** show optical images of selected glasses showing the spinel crystals above the accumulated layer after double crucible test at 850 °C for ~7 d. Well separated crystals with a size ~80 µm formed in the high-chromium glass (Cr0.3), Figure 7I. In contrast, agglomerates >130 µm formed in the high-nickel (Ni1.29) and high-nickel-chromium (Ni1.5/Cr0.3) glasses (Figures 7II and III, respectively). The agglomeration was even more pronounced in the high-nickel-iron (Ni1.5/Fe17.5) glass, Figure 7IV, because of the crystallization of larger number of crystals. Figure 8 illustrates the effect of RuO_2 addition to the high-nickel glass (Ni1.5) on the size and number density of crystals. A large number of micrometer-sized spinel crystals formed in the Ni1.5/Ru0.015 glass. Figure 9 shows the spinel dendrites that formed in the high-nickel-aluminum (Ni1.5/Al10) and high-nickel-lithium (Ni1.5/Li3.8) glasses (Figures 9I and II, respectively) during a period of fast cooling from 1200 to 850 °C. In contrast, the dendrites did not form in these glasses when slowly cooled at rates 1, 5, and 10°C/ min over the same temperature range. Since this rapid change in temperature is not expected in between periods of melter running and idling these needles-dendrites may not form in the riser.

The effect of NiO and noble metals on the crystal morphology agreed well with morphologies of crystals from previously tested glasses.[5,16] Interestingly, an increase in iron oxide concentration in Ni1.5/Fe17.5 glass from 17.5 mass% to 20 mass % resulted in the formation of dendrites observed after adding extra aluminum or lithium to Ni1.5 glass.

4.3 Accumulation of Spinel Crystals

Figure 10 shows the accumulation rates for spinel layer in the glasses that were heat-treated in double crucibles at 850°C for various times. The results for previously tested baseline (BL) and high-nickel (Ni1.5) glasses[5,16] were added to the graph for comparison. The baseline glass contained NiO at 0.64 mass%, Cr_2O_3 at 0.17 mass%, and Fe_2O_3 at 14.51 mass%, while Ni1.5 glass contained NiO at 1.5 mass%, Cr_2O_3 at 0.17 mass%, and Fe_2O_3 at 14.38 mass%. Table 7 shows the slopes and intercepts from the least squares linear fits to the data shown in Figure 8.

Adding 0.13 mass% of Cr_2O_3 to the baseline increased the accumulation rate of spinel from ~0.8 ± 0.0 to 1.5 ± 0.1 nm/s. Doubling the concentration of NiO in the baseline to 1.29 mass% (Ni1.29 glass) increased the accumulation rate ~4.5 times to ~3.6 ± 0.2 nm/s. An additional increase of NiO concentration to 1.5 mass% (Ni1.5 glass) resulted in the accumulation rate ~7.2 ± 0.5 nm/s, approximately 9 times faster than that for the baseline glass. This rate was more than doubled to ~14.9 ± 1.0 nm/s when ~3 mass% of Fe_2O_3 was added to the Ni1.5 glass (Ni1.5/Fe17.5 glass). In contrast, adding 0.13 mass% of Cr_2O_3 or 0.015 mass% of RuO_2 to Ni1.5 glass (Ni1.5/Cr0.3 or Ni1.5/Ru0.015 glass) decreased this rate to ~6.6 ± 0.6 or 0.06 ± 0.01 nm/s, respectively. More than twofold decrease in the accumulation rate for the Ni1.5/Ru0.015 glass demonstrates the high effectiveness of RuO_2 in slowing spinel accumulation. This was confirmed when an addition of RuO_2 at 0.087 mass% to the Ni1.5 glass (Ni1.5/Ru0.087) completely stopped the spinel accumulation.

Figure 11 shows the time-sequence SEM images of Ni1.5/Fe17.5 glass after heat-treatments at 850 °C, visualizing the growth of spinel sludge layer over the time as well as the size and concentration of crystals. Figure 12 provides a 3D projection of spinel agglomerates in the Ni1.5/Fe17.5 glass after heat-treatment at 850 °C for ~5 d. Cyan-colored features of agglomerates are located on the surface and black-colored features in the bulk of the glass. Platelets of hematite that were identified in this glass encouraged the formation of agglomerates > 500 µm.

Figure 13 shows accumulated layers in the Ni1.5/Ru0.015, Cr0.3, Ni1.29, and Ni1.5/Cr0.3 glasses that were heat-treated at 850 °C for ~7 d. The crystals up to 25 µm in size were found in the Ni1.5/Ru0.015 glass with ~25% > 10 µm. The average crystal size was 8.4 ± 9.9 µm. In contrast, all the crystals in the Cr0.3 glass were >14 µm. Also, the average and maximum size of crystals was 49.4 ± 50.3 and 110 µm, respectively. Crystals formed in the Ni1.29 glass were more than two times the size of the crystals found in the Cr0.3 glass, 116.1 ± 120.9 and 294 µm, because of agglomeration (see Figure 7III) and fast crystal growth. Also, about half of the crystals in the layer were >100 µm. Similar large single crystals and agglomerates were observed in the Ni1.5/Cr0.3 glass (Figure 7II), but their average and maximum size was 127.4 ± 139.9 and 354 µm, respectively.

Figure 14 shows dendrites of spinel that formed in the Ni15/Al10 and Ni1.5/Li3 glasses during heat-treatment at 850 °C for ~7 d. Crystals in these glasses did not form a compacted settled layer because of an extensive network of interconnected spinel dendrites. The area fraction of the crystals in the layers did not change with time and was less than 8%. Figure 15 details the size of spinel in the crystal clouds observed in the Ni1.5/Ru0.087 glass after 7 d of heat-treatment at 850 °C. An average crystal size varied from 3 ± 2.6 µm (Figure 15I) to 4.9 ± 4.9 µm (Figure 15II) and the maximum size of crystals was ~10 µm.

Points marked by dot circles in Figure 10 represent a post-settling period in Ni1.29, Ni1.5/Cr0.3, and Ni1.5/Fe17.5 glasses. In this period, the accumulation rate of spinel crystals was slower than in the linear-settling period because fewer and smaller crystals were available for settling. This is illustrated in Figure 16, which shows the layer of spinel accumulated in Ni1.5/Cr0.3 glass after ~14 d at 850 °C. The highlighted area at the top contains crystals with an average and maximum sizes 99 ± 104 and 287 µm, respectively. In contrast, the average and maximum sizes of the crystals that settled during the linear-settling period (middle section of Figure 16) were 140 ± 163 and 565 µm, respectively. The pre-settling period is represented by highlighted area at the bottom of Figure 16. In this period, crystals with an average size 56 ± 78 µm accumulated in the layer. Their small size compared to crystals at the top and middle sections is the result of crystals formed close to the bottom during cooling. EDS analysis of surrounding glass confirmed that these crystals grew slowly or stopped growing because the glass in their vicinity was depleted from spinel constituents.

4.4 Empirical Model of Spinel Settling

Previously, we developed an empirical model for spinel settling[16] with coefficients h_i and s_i expressed as a linear function of the mass fractions of seven major components in glass (Al_2O_3, Cr_2O_3, Fe_2O_3, ZnO, MnO, NiO, and others) to calculate crystal accumulation in the glass discharge riser of a HLW melter:

$$h = \sum_{i=1}^{7} h_i x_i + t \sum_{i=1}^{7} s_i x_i \qquad (2)$$

where h_i is a compositional dependent intercept coefficient (µm), t is the settling time (h), and s_i is a compositional dependent velocity coefficient (µm/h).

In this study, additional spinel-layer-thickness data were generated to refine the values of the model parameters. Specifically, the previous experimental data set was expanded with thicknesses of accumulated layers observed in Ni1.5/Cr0.3, Cr0.3 and Ni1.29 glasses. Table 8 shows the calculated coefficients h_i and s_i, the values of R^2 (expresses the fraction of the variability accounted for by the model), and R^2_{adj} (adjusts R^2 for the number of parameters used in fitting the model). The positive coefficients s_i for MnO, ZnO, Cr_2O_3, and NiO indicate that these components increase the rate of accumulation. In contrast, additions of Al_2O_3 and Fe_2O_3 decrease the accumulation rate. Also, our experiments showed that the detrimental effect of the most troublesome component (NiO) on the accumulation rate can be significantly suppressed by the addition of trace amounts of RuO_2 to the glass.

In Figure 17, we show the calculated and the measured thicknesses of a spinel sludge layer for the glasses used in the model fit and for Ni1.5/Fe17.5 glass. With these parameter values, we calculate the accumulation of crystals in the glasses with no or small-scale agglomeration, in which spinel settles as individual crystals and/or as clusters of a few crystals. There is a good comparison between the calculated and the observed accumulation. But, in the case of excessive agglomeration that was observed for the Ni1.5/Fe17.5 glass, the model under-predicts the thicknesses of deposited layers. The agreement became poorer with time as an increased number of larger agglomerates formed. Another factor that affected greatly the accumulation of spinel was the formation of 3D network of spinel dendrites in the Ni1.5/Al10 and Ni1.5/Li.38 glasses that prevented the formation of a dense settled layer. Since dense layers did not form in these glasses, they were excluded from model fitting. Additionally, we were unable to detect continuous accumulated layers of spinel in the Ni1.5/Ru0.015 glass, and therefore, did not use these data.

4.5 Particle Agglomeration

A question arises whether it would be possible to control the accumulation rate of spinel crystals through optimization of the noble metals concentration in radioactive wastes. A small concentration of noble metals may be sufficient to nucleate enough spinel crystals to limit their growth to a size of ≤10 µm. However, high concentrations of noble metals are unfavorable because of their tendency to form large agglomerates.[20] These rapidly settling agglomerates can also form due to interactions of spinel crystals with noble metal particles. Therefore, we used X-ray tomography and SEM-EDS to investigate particle agglomeration (size and concentration of agglomerates) and accumulation rates in two HLW glasses.

Figure 18 shows agglomerates (white specs) in slices collected in the middle of and perpendicular to the vertical axis of the crucible for BL/RuO2 (A) and Ni1.5/Ru02 (B) glasses that were heat-treated at 850 °C for ~2 d. The BL/RuO2 contained 44 agglomerates of maximum and average sizes 412 and 111 ± 159 µm, respectively. In contrast, Ni1.5/RuO2 contained 41 agglomerates of maximum and average sizes 138 and 68 ± 64 µm, respectively. These results suggest that significantly larger agglomerates formed in the BL/RuO2. However, the overall size distribution of agglomerates was not significantly different. The averages of maximum and average sizes in the BL/RuO2 were 167 ± 38 and 94 ± 12 µm, respectively, compared to 148 ± 33 and 86 ± 9 µm in the Ni1.5/RuO2. Also, the number density of agglomerates was about the same; 1100 ± 300 and 1000 ± 300 per mm^2 in the BL/RuO2 and Ni1.5/RuO2 glasses, respectively. In addition, we did not observe an accumulation layer in any of these glasses even after 4 d at 850 °C, indicating that agglomerates of this size and shape (Figures 21 and 22) settle slowly.

Figure 19 shows agglomerates in horizontal xy-slices collected at 16 (I) and 26 mm (II) above the bottom for Ni1.5/Ru02 glass heat-treated at 850 °C for ~2 d. About 17 agglomerates were detected closer to the bottom with maximum and average sizes 153 and 95 ± 73 µm, respectively. The higher number (27) and larger agglomerates were detected further from the bottom (maximum and average sizes 178 and 101 ± 93 µm, respectively). Figure 20 and Figure 21 shows maximum and average size of agglomerates as a function of the distance from the bottom of the crucible for BL/RuO2 and Ni1.5/RuO2 glasses heat-treated at 850 °C for ~2 d. The linear fit of the data indicates a gradual increase in the averages of maximum and average sizes of agglomerates from bottom to the top for tested glasses. This increase is similar in both glasses except for more than 3 times higher increase in maximum size for agglomerates in the Ni1.5/RuO2.

Figure 22 shows in detail the shape and size of the agglomerates that formed in the Ni1.5/RuO2 glass heat-treated at 850 °C for A) ~2 d, B) ~3 d, and C) ~4 d. Figure 23 shows the same for BL/RuO2. The SEM analysis results confirmed that the size of agglomerates increased with time and were consistent with the results from X-ray tomography.

5. Conclusions

The experimental study of spinel accumulation confirmed that high concentrations of spinel-forming constituents in the glass can produce settled layers of a few cm thick in a few weeks. An excessive agglomeration of spinel in high-Ni-Fe glass (Ni1.5/Fe17.5) with agglomerates >500 µm resulted in the accumulation rate 14.943 ± 1.016 nm/s that can produce a 26 mm-thick layer in just 20 days of melter idling and potentially plug the riser. Our data indicate that noble metals can significantly decrease the accumulation rate of spinel crystals. Additions of RuO_2 (in the form of ruthenium nitrosyl nitrate) to high-Ni glass (Ni1.5) effectively slowed or stopped spinel accumulation because of their effect on decreasing the average crystal size below 10 µm. High concentration of spinel dendrites in high-nickel glasses containing extra Al_2O_3 and Li_2O prevented the formation of dense layers. However, these dendrites may not form in the riser because a period of fast cooling is not expected in between periods of melter running and idling.

Developed empirical settling model predicts well the accumulation of crystals in the glasses with no or small-scale agglomeration, in which spinel settles as individual crystals and/or as clusters of a few crystals. But, more experimental data are needed to make the model more robust and useful in accounting for the effects of agglomeration and different crystal morphologies on accumulation rate and structure (dense vs. non-compacted) of the layer.

From the agglomeration tests on two glasses of different compositions enriched with Rh_2O_3 and RuO_2, we have learned that spinel and RuO_2 agglomerates > 100 µm slowly settle because of their size and shape. These non-compact agglomerates were composed of loosely contacting particles that resulted in high-surface area agglomerates with “holes.” The X-ray tomography combined with SEM and image analysis also revealed that the size of agglomerates slowly increased with time and distance from the bottom of the crucible.

6. Acknowledgements

The authors would like to thank U.S. Department of Energy's Hanford Tank Waste Treatment and Immobilization Plant Federal Project Office, Engineering Division, for financial support. The authors would also like to acknowledge Michael Schweiger for laboratory assistance, Pavel Hrma for insightful conversations and Denis Strachan for his helpful suggestions and comments on the manuscript. Pacific Northwest National Laboratory is operated by Battelle for the U.S. Department of Energy under Contract DE-AC05-76RL01830.

7. References

[1] D.-S. Kim and J. D. Vienna. 2002. “Influence of Glass Property Restrictions on Hanford Glass Volume,” In *Proceedings of the Ceramic Transactions: Environmental Issues and Waste*

*Management Technologies in the Ceramic and Nuclear Industries VII:*103rd *Annual Meeting of ACerS:* held in Indianapolis, Indiana, USA, April 22-25, 2001, **132**. pp. 105-115, Edited by G. L. Smith, S. K. Sundaram, and D. R. Spearing. The American Ceramic Society, Westerville, OH.

[2] P. Hrma, J. Matyáš, and D.-S. Kim. 2003. "Evaluation of Crystallinity Constraint for HLW Glass Processing," In *Proceedings of the Ceramic Transactions: Environmental Issues and Waste Management Technologies in the Ceramic and Nuclear Industries VIII:*104th Annual Meeting of ACerS: held in St. Louis, Missouri, USA, April 28-30, 2002, **143**. pp. 133-140, Edited by S. K. Sundaram, D. R. Spearing, and J. D. Vienna. The American Ceramic Society, Westerville, OH.

[3] J. Matyáš, J. Kloužek, L. Němec, and M. Trochta. 2002. "Spinel Settling in HLW Melters," In *Proceedings of the 8th International Conference on Radioactive Waste Management and Environmental Remediation: ICEM'01*: held in Bruges, Belgium, September 30-October 4, 2001, **3**, pp. 1787-1792, Edited by A. Taboas, R. Vanbrabant, and G. Benda. The American Society of Mechanical Engineers, New York, NY.

[4] P. Izak, P. Hrma, B. W. Arey, and T. J. Plaisted. "Effect of Feed Melting, Temperature History, and Minor Component Addition on Spinel Crystallization in High-Level Waste Glass," *J. Non-Cryst. Solids*, **289** [1-3], 17-29 (2001).

[5] J. Matyáš, J. D. Vienna, A. Kimura, M. Schaible, and R. M. Tate. 2010b. "Development of Crystal-Tolerant Waste Glasses," In *Proceedings of the Ceramic Transactions: Advances in Material Science for Environmental and Nuclear Technology: MS&T'09*, held in Pittsburgh, Pennsylvania, USA, October 25-29, 2009, **222**. pp. 41-51, Edited by K. Fox,

E. Hoffamn, N. Manjooran, and G. Pickrell. The American Ceramic Society, Westerville, OH.

[6] M. Mika, P. Hrma, and M. J. Schweiger. "Rheology of Spinel Sludge in Molten Glass," *Ceramics-Silikaty*, **44** [3], 86–90 (2000).

[7] M. Mika, M. Liska, and P. Hrma. "The Effect of Spinel Sludge Aging on its Viscosity," *Ceramics-Silikaty*, **46** [4], 148–151 (2002).

[8] M. W. Stachnik, P. Hrma, and H. Li. 2000. "Effects of High-level Waste Glass Composition on Spinel Precipitation," In *Proceedings of the Ceramic Transactions: Environmental Issues and Waste Management Technologies in the Ceramic and Nuclear Industries V:* 101st Annual Meeting of ACerS: held in Indianapolis, Indiana, USA, April 25-28, 1999, **107**. pp. 123-130, Edited by G. T. Chandler and X. Feng. The American Ceramic Society, Westerville, OH.

[9] B. K. Wilson, P. Hrma, J. Alton, T. J. Plaisted, and J. D. Vienna. "The Effect of Composition on Spinel Equilibrium and Crystal Size in High-Level Waste Glass," *Journal of Material Science*, **37** [24], 5327–5311 (2002).

[10] M. Jiricka, P. Hrma, and J.D. Vienna. "The Effect of Composition on Spinel Crystals Equilibrium in Low-Silica High-Level Waste Glasses," *J. Non-Cryst. Solids*, **319** [3], 280–288 (2003).

[11] J. Alton, T. J. Plaisted, and P. Hrma. "Dissolution and Growth of Spinel Crystals in a Borosilicate Glass," *J. Non-Cryst. Solids*, **311** [1], 24–35 (2002).

[12] J. Alton, T. J. Plaisted, and P. Hrma. "Kinetics of Growth of Spinel Crystals in a Borosilicate Glass," *Chemical Engineering Science*, **57** [13], 2503–2509 (2002).

[13] J. LaMont and P. Hrma. 1998. “A Crucible Study of Spinel Settling in a High-Level Waste Glass,” In *Proceedings of the Ceramic Transactions: Environmental Issues and Waste Management Technologies in the Ceramic and Nuclear Industries III:* 99th Annual Meeting of ACerS: held in Cincinnati, Ohio, USA, May 4-7, 1997, **87**. pp. 343–348, Edited by D. K. Peeler and J. C. Mara. The American Ceramic Society, Westerville, OH.

[14] J. Kloužek, J. Alton, T. J. Plaisted, and P. Hrma. 2001. “Crucible Study of Spinel Settling in High-Level Waste Glass,” In *Proceedings of the Ceramic Transactions: Environmental Issues and Waste Management Technologies in the Ceramic and Nuclear Industries VI*: 102nd Annual Meeting of ACerS: held in St. Louis, Missouri, USA, April 25-May 3, 2000, **119**. pp. 301–308, Edited by D. R. Spearing and G. L. Smith, and R. L Putman. The American Ceramic Society, Westerville, OH.

[15] K. S. Matlack, W. K. Kot, W. Gong, W. Lutze, I. L. Pegg, and I. Joseph. 2009. *Effects of High Spinel and Chromium Oxide Crystal Contents on Simulated HLW Vitrification in DM100 Melter Tests*. VSL 09R1520-1, U.S. Department of Energy Office of River Protection, Richland, Washington.

[16] J. Matyáš, J. D. Vienna, M. J. Schaible, C. P. Rodriquez, and J. V. Crum. 2010. *Development of Crystal-Tolerant High-Level Waste Glasses*. PNNL-20072, Pacific Northwest National Laboratory, Richland, Washington.

[17] J. Matyáš, J. D. Vienna, and M. J. Schaible. 2011. “Determination of Stokes Shape Factor for Single Particles and Agglomerates,” In *Proceedings of the Ceramic Transactions: Advances in Material Science for Environmental and Nuclear Technology II: MS&T'10,* held in Houston, Texas, USA, October 17-21, 2010, **227**. pp. 195–203, Edited by S. K.

Sudaram, T. Ohji, K. Fox, and E. Hoffman. The American Ceramic Society, Westerville, OH.

[18] R. E. Eibling, R. F. Schumacher, and E. K. Hansen. 2003. *Development of Simulants to Support Mixing Tests for High Level Waste and Low Activity Waste*, SRT-RPP-2003-00098, REV. 0, Westinghouse Savannah River Company, Aiken, South Carolina.

[19] ASTM C 1720-11, 2011. *Standard Test Method for Determining Liquidus Temperature of Immobilized Waste Glasses and Simulated Waste Glasses*, American Society for Testing and Materials, West Conshohocken, PA.

[20] K. M. Fox, D. K. Peeler, T. B. Edwards, D. R. Best, I. A. Reamer, R. J. Workman, J. C. Marra, B. J. Riley, J. D. Vienna, J. V. Crum, J. Matyáš, A. B. Edmondson, J. B. Lang, N. M. Ibarra, A. Fluegel, A. Aloy, A. V. Trofimenko, and R. Soshnikov. 2008. *International Study of Aluminum Impacts on Crystallization in U.S. High Level Waste Glass*, SRNS-STI-2008-00057, Savannah River National Laboratory, Aiken, South Carolina.

List of Tables

Table 1. Target composition of HLW AZ-101 simulant[18] in mass fraction of oxides and halogens.

Component		Component		Component		Component	
Al_2O_3	0.2263	Fe_2O_3	0.3999	Rh_2O_3	NA	Cl	0.0006
B_2O_3	0.0159	K_2O	0.0095	RuO_2	NA	Ce_2O_3	0.0056
BaO	0.0026	MgO	0.0036	SiO_2	0.0467	CoO	0.0003
CaO	0.0158	MnO	0.0097	SO_3	0.0023	CuO	0.0011
CdO	0.0178	Na_2O	0.0786	TiO_2	0.0008	La_2O_3	0.0061
Cr_2O_3	0.0047	NiO	0.0175	ZnO	0.0006	Nd_2O_3	0.0050
F	0.0002	P_2O_5	0.0088	ZrO_2	0.1148	SnO_2	0.0027

NA = Noble metals were not added.

Table 2. Analyzed composition of HLW AZ-101 simulant compared with target composition of simulant from literature[18].

Component	AZ-101 (Eibling et al. 2003)	AZ-101 (Analyzed)(a)	Average	SD	RSD, %	RPD, %
Al_2O_3	0.2263	0.2022	0.2143	0.0170	8.0	-10.6
B_2O_3	0.0159	0.0012	0.0086	0.0104	120.9	-92.5
BaO	0.0026	0.0019	0.0023	0.0005	21.5	-26.9
CaO	0.0158	0.0116	0.0137	0.0030	21.7	-26.6
CdO	0.0178	0.0172	0.0175	0.0004	2.4	-3.4
Cr_2O_3	0.0047	0.0036	0.0042	0.0008	18.5	-23.4
F	0.0002	NA	-	-	-	-
Fe_2O_3	0.3999	0.3231	0.3615	0.0543	15.0	-19.2
K_2O	0.0095	0.0034	0.0065	0.0043	66.4	-64.2
MgO	0.0036	0.0028	0.0032	0.0006	17.7	-22.2
MnO	0.0097	0.0078	0.0088	0.0013	15.3	-19.6
Na_2O	0.0786	0.0847	0.0817	0.0043	5.3	7.8
NiO	0.0175	0.0131	0.0153	0.0031	20.3	-25.1
P_2O_5	0.0088	0.0081	0.0085	0.0005	5.8	-8.0
Rh_2O_3	0.0009	2.5E-07	-	-	-	-
RuO_2	0.0017	1.2E-06	-	-	-	-
SiO_2	0.0467	0.0320	0.0394	0.0104	26.4	-31.5
SO_3	0.0023	0.0012	0.0018	0.0008	43.2	-47.8
TiO_2	0.0008	0.0004	0.0006	0.0003	47.1	-50.0
ZnO	0.0006	0.0004	0.0005	0.0001	28.3	-33.3
ZrO_2	0.1148	0.0933	0.1041	0.0152	14.6	-18.7
Cl	0.0006	NA	-	-	-	-
Ce_2O_3	0.0056	NA	-	-	-	-
CoO	0.0003	0.0002	0.0003	0.0001	23.6	-33.3
CuO	0.0011	0.0008	0.0010	0.0002	21.2	-27.3
La_2O_3	0.0061	0.0075	0.0068	0.0010	14.6	23.0
Nd_2O_3	0.0050	NA	-	-	-	-
SnO_2	0.0027	0.0040	0.0034	0.0009	27.0	48.1
LOI	-	0.1607	-	-	-	-
Total	1.0000	0.9812	-	-	-	-

(a) Does not include 0.0019 PbO, 9.0×10^6 Li_2O, and 0.0001 MoO_3; - = Empty field; LOI = Loss on ignition at 1000°C; NA = Not analyzed; RPD = Relative percent difference between analyzed and literature compositions; RSD = Relative standard deviation (SD/Average); SD = Standard deviation.

Table 3. Target composition of formulated glasses in mass fraction of oxides and halogens.

Component	BL	Ni1.29	Cr0.3	Ni1.5/Al10	Ni1.5/Fe17.5	Ni1.5/Li3.8	Ni1.5/Cr0.3	Ni1.5/Ru0.015(a)	Ni1.5/Ru0.087(b)
Al_2O_3	0.0821	0.0816	0.0820	0.1000	0.0784	0.0799	0.0813	0.0814	0.0813
B_2O_3	0.0799	0.0794	0.0798	0.0776	0.0763	0.0777	0.0791	0.0792	0.0791
BaO	0.0009	0.0009	0.0009	0.0009	0.0009	0.0009	0.0009	0.0009	0.0009
CaO	0.0057	0.0057	0.0057	0.0055	0.0054	0.0055	0.0056	0.0057	0.0056
CdO	0.0065	0.0065	0.0065	0.0063	0.0062	0.0063	0.0064	0.0064	0.0064
Cr_2O_3	0.0017	0.0017	0.0030	0.0017	0.0016	0.0017	0.0030	0.0017	0.0017
F	0.0001	0.0001	0.0001	0.0001	0.0001	0.0001	0.0001	0.0001	0.0001
Fe_2O_3	0.1451	0.1441	0.1448	0.1408	0.1750	0.1410	0.1436	0.1437	0.1436
K_2O	0.0034	0.0034	0.0034	0.0033	0.0032	0.0033	0.0034	0.0034	0.0034
Li_2O	0.0199	0.0198	0.0199	0.0193	0.0190	0.0380	0.0197	0.0197	0.0197
MgO	0.0013	0.0013	0.0013	0.0013	0.0012	0.0013	0.0013	0.0013	0.0013
MnO	0.0035	0.0035	0.0035	0.0034	0.0033	0.0034	0.0035	0.0035	0.0035
Na_2O	0.1866	0.1853	0.1864	0.1812	0.1781	0.1814	0.1847	0.1849	0.1847
NiO	0.0064	0.0129	0.0064	0.0150	0.0150	0.0150	0.0150	0.0150	0.0150
P_2O_5	0.0032	0.0032	0.0032	0.0031	0.0031	0.0031	0.0032	0.0032	0.0032
SiO_2	0.4031	0.4003	0.4025	0.3913	0.3847	0.3920	0.3989	0.3994	0.3991
SO_3	0.0008	0.0008	0.0008	0.0008	0.0008	0.0008	0.0008	0.0008	0.0008
TiO_2	0.0003	0.0003	0.0003	0.0003	0.0003	0.0003	0.0003	0.0003	0.0003
ZnO	0.0002	0.0002	0.0002	0.0002	0.0002	0.0002	0.0002	0.0002	0.0002
ZrO_2	0.0416	0.0413	0.0415	0.0404	0.0397	0.0405	0.0412	0.0412	0.0412
Cl	0.0002	0.0002	0.0002	0.0002	0.0002	0.0002	0.0002	0.0002	0.0002
Ce_2O_3	0.0020	0.0020	0.0020	0.0019	0.0019	0.0019	0.0020	0.0020	0.0020
CoO	0.0001	0.0001	0.0001	0.0001	0.0001	0.0001	0.0001	0.0001	0.0001
CuO	0.0004	0.0004	0.0004	0.0004	0.0004	0.0004	0.0004	0.0004	0.0004
La_2O_3	0.0022	0.0022	0.0022	0.0021	0.0021	0.0021	0.0022	0.0022	0.0022
Nd_2O_3	0.0018	0.0018	0.0018	0.0017	0.0017	0.0018	0.0018	0.0018	0.0018
SnO_2	0.0010	0.0010	0.0010	0.0010	0.0010	0.0010	0.0010	0.0010	0.0010
Total	1.0000	1.0000	1.0000	1.0000	1.0000	1.0000	1.0000	0.9996	0.9988

(a) Added 1.5×10^{-4} RuO_2 and 3×10^{-4} Rh_2O_3; (b) Added 8.7×10^{-4} RuO_2 and 3×10^{-4} Rh_2O_3.

Table 4. Target compositions of the glasses used in agglomeration study in mass fraction of oxides and halogens.

Component	BL/RuO_2	Ni1.5/RuO_2
Al_2O_3	0.0819	0.0812
B_2O_3	0.0797	0.0790
BaO	0.0009	0.0009
CaO	0.0057	0.0056
CdO	0.0065	0.0064
Cr_2O_3	0.0017	0.0017
F	0.0001	0.0001
Fe_2O_3	0.1446	0.1433
K_2O	0.0034	0.0034
Li_2O	0.0198	0.0197
MgO	0.0013	0.0013
MnO	0.0035	0.0035
Na_2O	0.1860	0.1844
NiO	0.0064	0.0150
P_2O_5	0.0032	0.0032
Rh_2O_3	0.0003	0.0003
RuO_2	0.0029	0.0029
SiO_2	0.4018	0.3983
SO_3	0.0008	0.0008
TiO_2	0.0003	0.0003
ZnO	0.0002	0.0002
ZrO_2	0.0415	0.0411
Cl	0.0002	0.0002
Ce_2O_3	0.0020	0.0020
CoO	0.0001	0.0001
CuO	0.0004	0.0004
La_2O_3	0.0022	0.0022
Nd_2O_3	0.0018	0.0018
SnO_2	0.0010	0.0010
Total	1.0000	1.0000

Table 5. Parameter values (C_{max}, B_L, $T_L^{(a)}$) from the least squares fit of experimental data to Eq. (1) and $T_L^{(b)}$ as determined from optical microscopy data.

Glass ID	C_{max}, mass fraction	B_L, K	$T_L^{(a)}$, °C	$T_L^{(b)}$, °C
Cr0.3	0.066 ± 0.154	2126 ± 5302	949 ± 4	950
Ni1.29	0.037 ± 0.005	12633 ± 3113	988 ± 4	1005
Ni1.5/Al10	0.051 ± 0.004	11687 ± 2213	1074 ± 6	1075
Ni1.5/Fe17.5	0.058 ± 0.005	13175 ± 3014	1125 ± 9	1105
Ni1.5/Li3.8	0.048 ± 0.011	10344 ± 4601	1012 ± 11	1004
Ni1.5/Cr0.3	0.043 ± 0.005	11726 ± 2789	1021 ± 4	1018
Ni1.5/Ru0.015	0.129 ± 0.390	2295 ± 8688	1051 ± 66	1087
Ni1.5/Ru0.087	0.119 ± 0.053	2452 ± 1293	1061 ± 5	1085

Table 6. Concentration of spinel in mass (C_0) and volume (V_0) percent for glasses heat-treated at 850 °C for 24 h.

Glass ID	C_0, mass%	V_0, vol%[(a)]
Cr0.3	0.9	0.5
Ni1.29	2.7	1.4
Ni1.5/Al10	4.1	2.1
Ni1.5/Fe17.5	5.3	2.7
Ni1.5/Li3.8	3.3	1.7
Ni1.5/Cr0.3	3.3	1.7
Ni1.5/Ru0.015	3.5	1.8
Ni1.5/Ru0.087	3.4	1.7

(a) For $C_0 \langle\langle 1$, the volume percent of spinel is $V_0 \cong C_0 \rho_g / \rho_s$, where ρ_g is the glass density (2.7×10^3 kg/m^3) and ρ_s is the spinel density (5.3×10^3 kg/m^3).

Table 7. Slope (A) and intercept (B) from the linear least squares fit of the data shown in Figure 10.

Glass ID	A, nm/s	B, 10^3 nm	R^2
BL(a)	0.817 ± 0.028	-196.0 ± 25.2	0.99
Ni1.5(a)	7.192 ± 0.457	-1951.36 ± 273.4	0.98
Ni1.29	3.603 ± 0.185	-507.39 ± 134.1	1.00
Cr0.3	1.453 ± 0.110	-691.66 ± 95.2	0.99
Ni1.5/Fe17.5	14.943 ± 1.016	-2321.20 ± 432.5	0.99
Ni1.5/Cr0.3	6.568 ± 0.629	-1691.97 ± 358.2	0.99
Ni1.5/Ru0.015	0.062 ± 0.007	-4.69 ± 6.3	0.99

(a) Previously tested glasses[5,16]

Table 8. Component coefficients calculated with the empirical model of spinel settling Eq. 2[16].

Components	h_i (μm)	s_i (μm/h)
Al_2O_3	9206	-339
Fe_2O_3	4895	-52
MnO	7734	189
ZnO	-15287	342
Cr_2O_3	-62253	520
NiO	-176907	2498
Others	-768	28
R^2	0.981	
R^2 adj	0.968	

List of Figures

Figure 14. Backscattered electron SEM images of spinel dendrites for glasses heat-treated at 850 °C: I) Ni15/Al10 glass, 167 h 40 min and II) Ni1.5/Li3.8 glass, 169 h.

Figure 15. Backscattered electron SEM images of crystal clouds for Ni1.5/Ru0.087 glass heat-treated at 850 °C for 168 h. An average size of crystals for image I) and II) was 3±2.6 µm and 4.9±4.9 µm, respectively.

Figure 16. Backscattered electron SEM images of accumulated spinel layer for Ni1.5/CrO.3 glass heat-treated at 850 °C for 332 h. Top and bottom highlighted areas represent post-settling and pre-settling period, respectively.

Figure 17. Calculated vs. measured thicknesses of accumulated layers for the glasses used in the model fitting (red diamonds) and for Ni1.5/Fe17.5 Glass (green stars).

Figure 18. X-Ray tomograph images of agglomerates (white specs) in the XZ Slice in the Middle of the alumina crucible for glasses heat-treated at 850 °C: I) BL/$Ru0_2$ glass, 48 h and II) Ni1.5/$Ru0_2$ glass, 45 h 15 min; walls of alumina crucible are dark grey, gray areas are glass, black rounded features are cavities and black lines are cracks.

Figure 19. X-Ray tomograph images of agglomerates (white specs) developed in the Ni1.5/$Ru0_2$ glass (gray areas) heat-treated at 850 °C for 45 h 15 min: I) XY slice 16 mm above the bottom and II) XY slice 26 mm above the bottom; alumina crucible is dark gray circle, gray areas are glass.

Figure 20. Maximum and average size of agglomerates as a function of the distance from the bottom of the crucible for BL/RuO2 glass heat-treated at 850 °C for 48 h. The solid lines are linear fit of the data (maximum size: $y = 5.6 \pm 7.6x+158.5 \pm 13.3$ and average size: $y = 5.1 \pm 2.1x+86.4 \pm 3.8$).

Figure 21. Maximum and average size of agglomerates as a function of the distance from the bottom of the crucible for Ni1.5/RuO2 glass heat-treated at 850 °C for 45 h 15 min. The solid lines are linear fit of the data (maximum size: $y = 17.1 \pm 6.1x+122.4 \pm 10.6$ and average size: $y = 5.3 \pm 1.6x+78.3 \pm 2.7$).

Figure 22. Backscattered electron SEM images of particle agglomerates for Ni1.5/RuO_2 glass heat-treated at 850 °C for I) 45 h 15 min, II) 74 h 45 min. Spinel crystals are gray features, RuO_2 white specs, and glass is dark gray.

Figure 23. Backscattered electron SEM images of particle agglomerates for BL/RuO_2 glass heat-treated at 850 °C for I) 48 h and II) 93 h 25 min. Spinel crystals are gray features, RuO_2 white specs, and glass is dark gray.

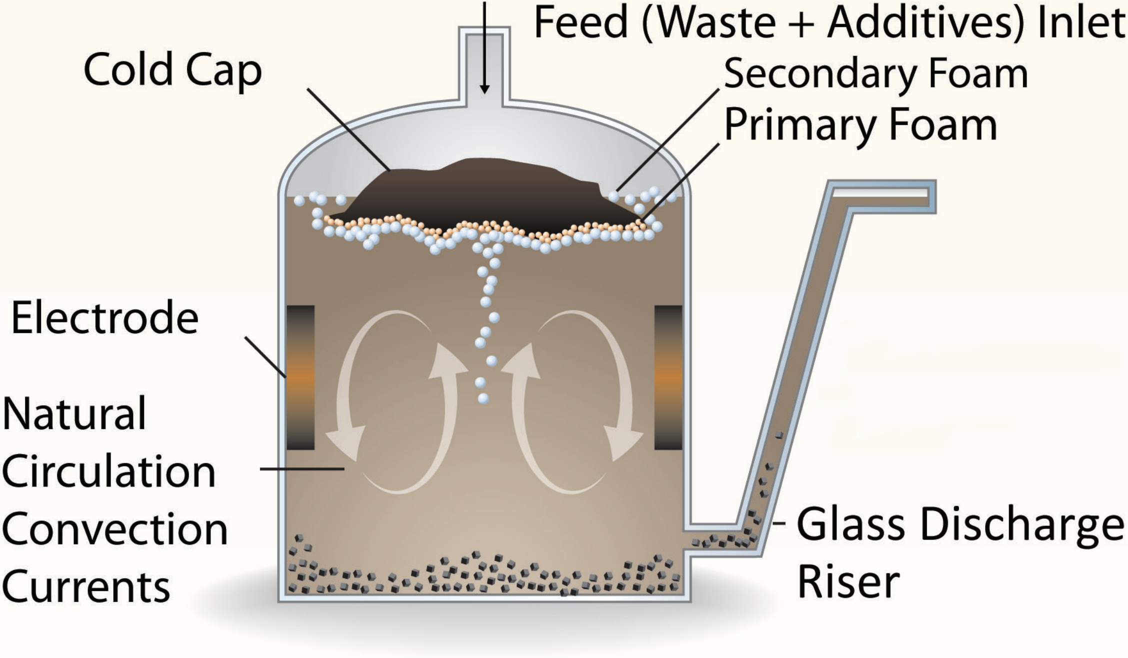
Feed (Waste + Additives) Inlet
Cold Cap
Secondary Foam
Primary Foam
Electrode
Natural Circulation Convection Currents
Glass Discharge Riser

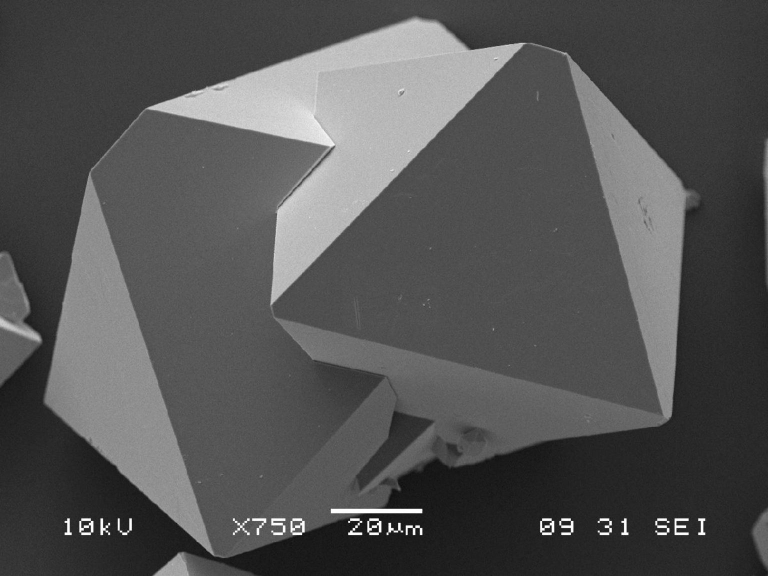
10kV
X750
20µm
09 31 SEI

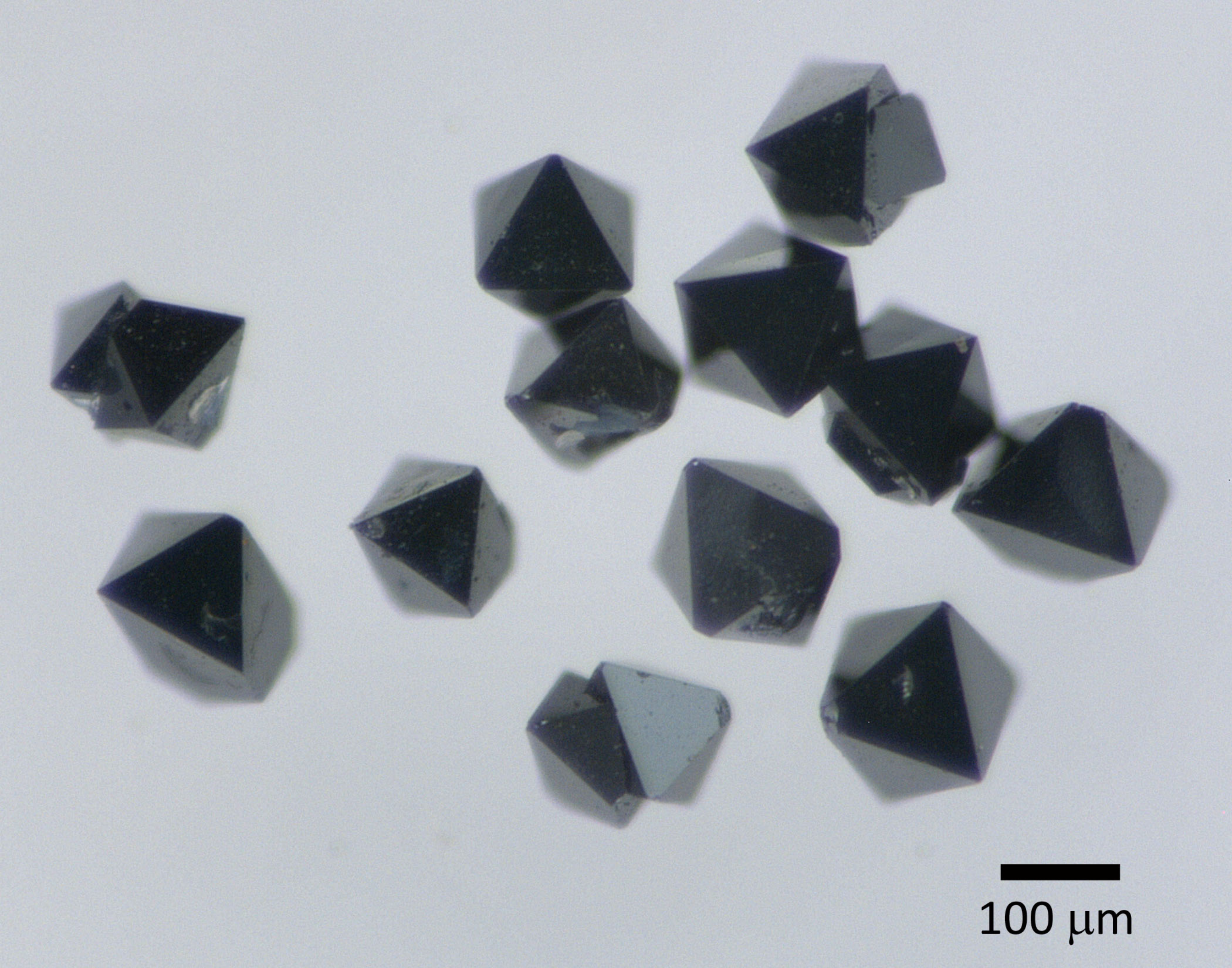
100 μm

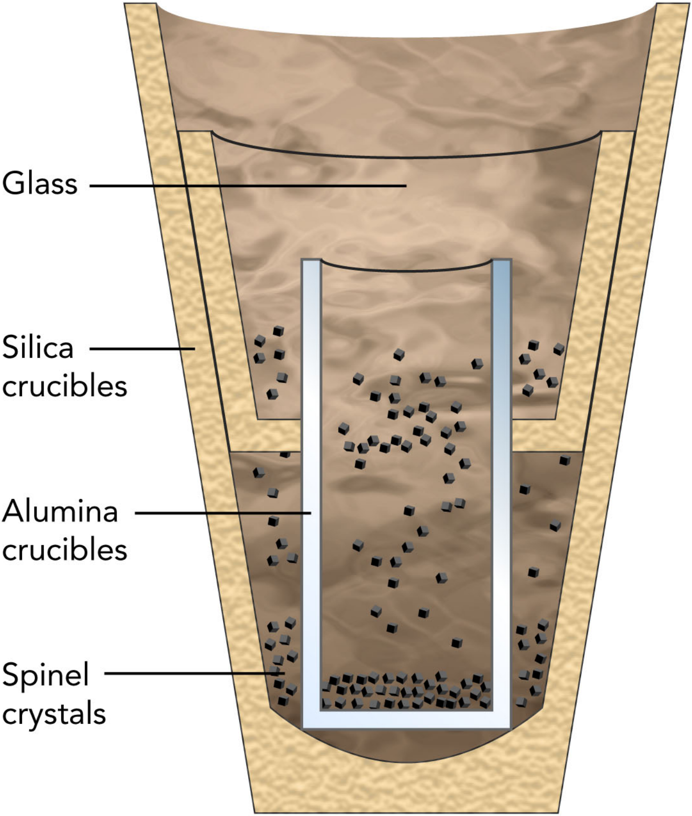

Glass
Silica crucibles
Alumina crucibles
Spinel crystals

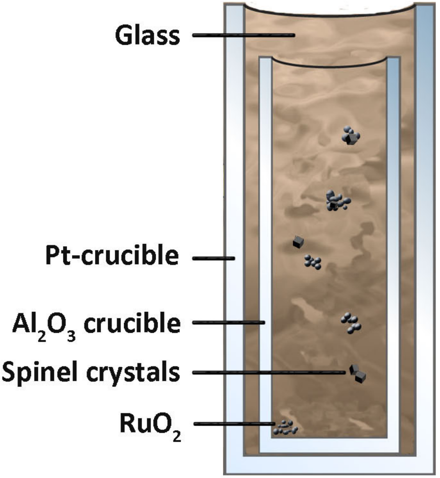
Glass
Pt-crucible
Al_2O_3 crucible
Spinel crystals
RuO_2

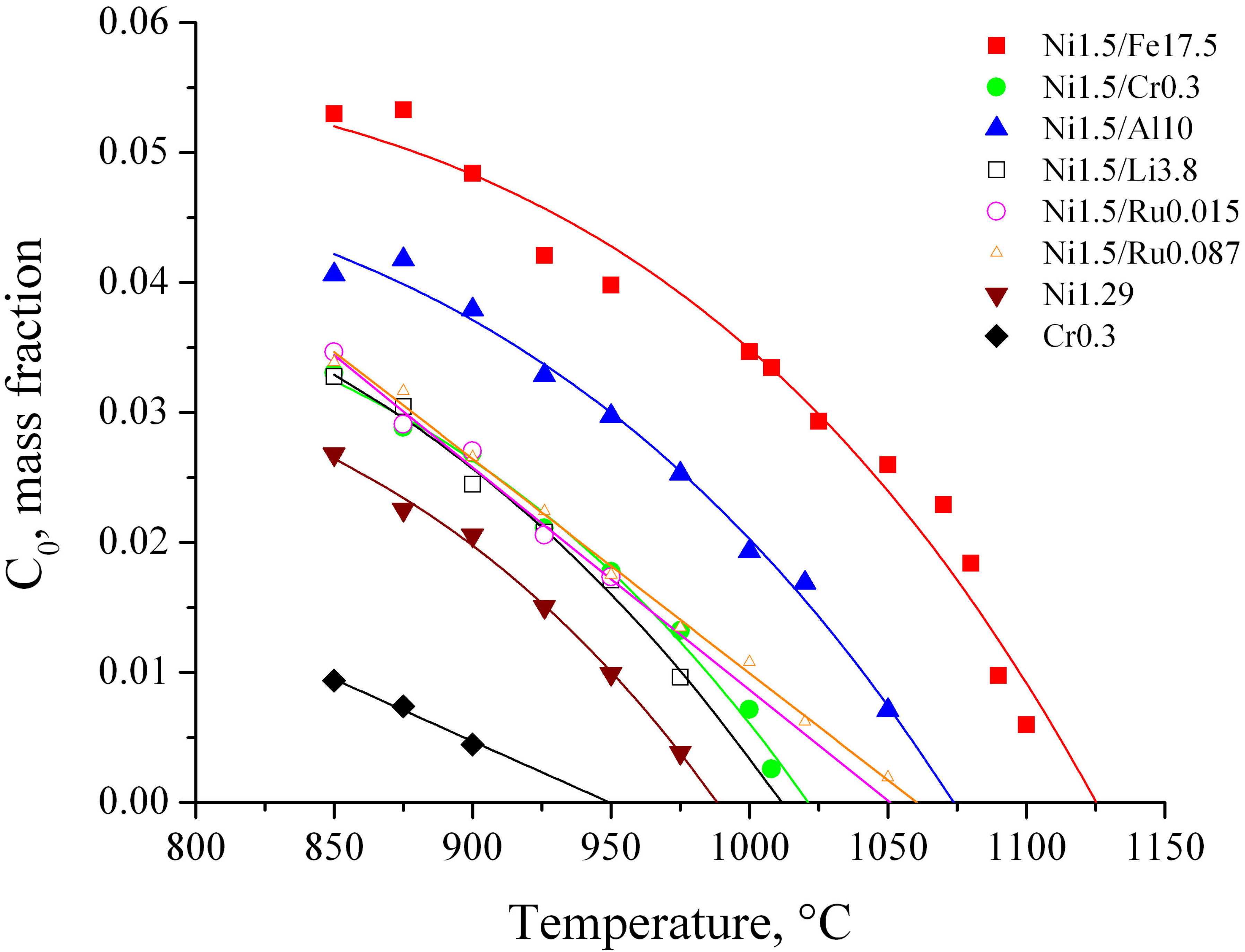
C$_0$, mass fraction
0.00
0.01
0.02
0.03
0.04
0.05
0.06
Temperature, °C
800
850
900
950
1000
1050
1100
1150
Ni1.5/Fe17.5
Ni1.5/Cr0.3
Ni1.5/Al10
Ni1.5/Li3.8
Ni1.5/Ru0.015
Ni1.5/Ru0.087
Ni1.29
Cr0.3

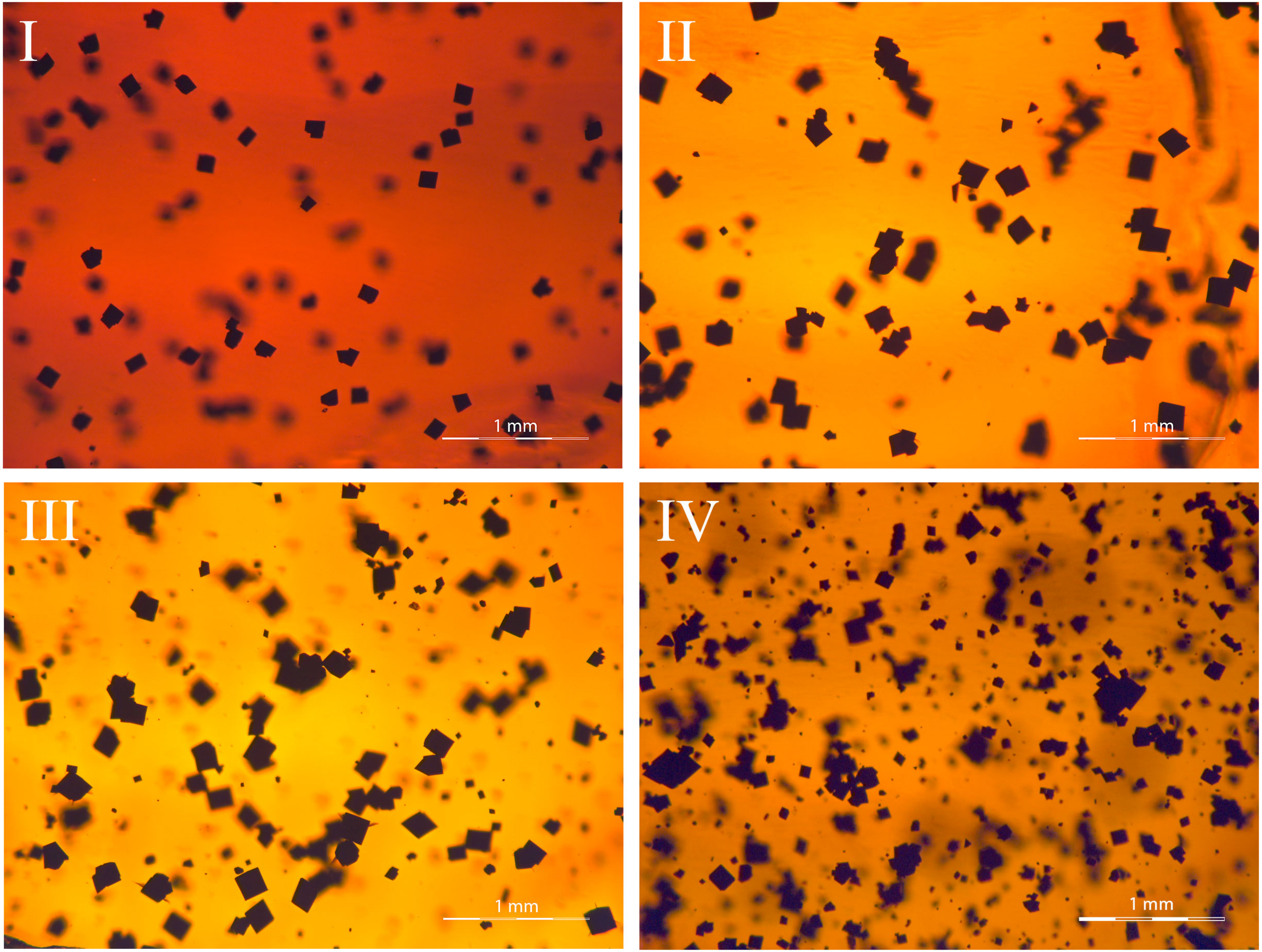
I
1 mm
II
1 mm
III
1 mm
IV
1 mm

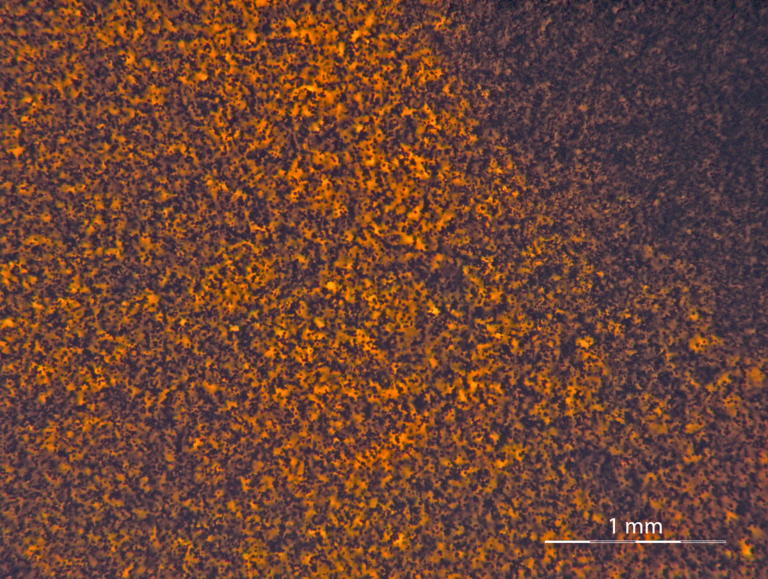
1 mm

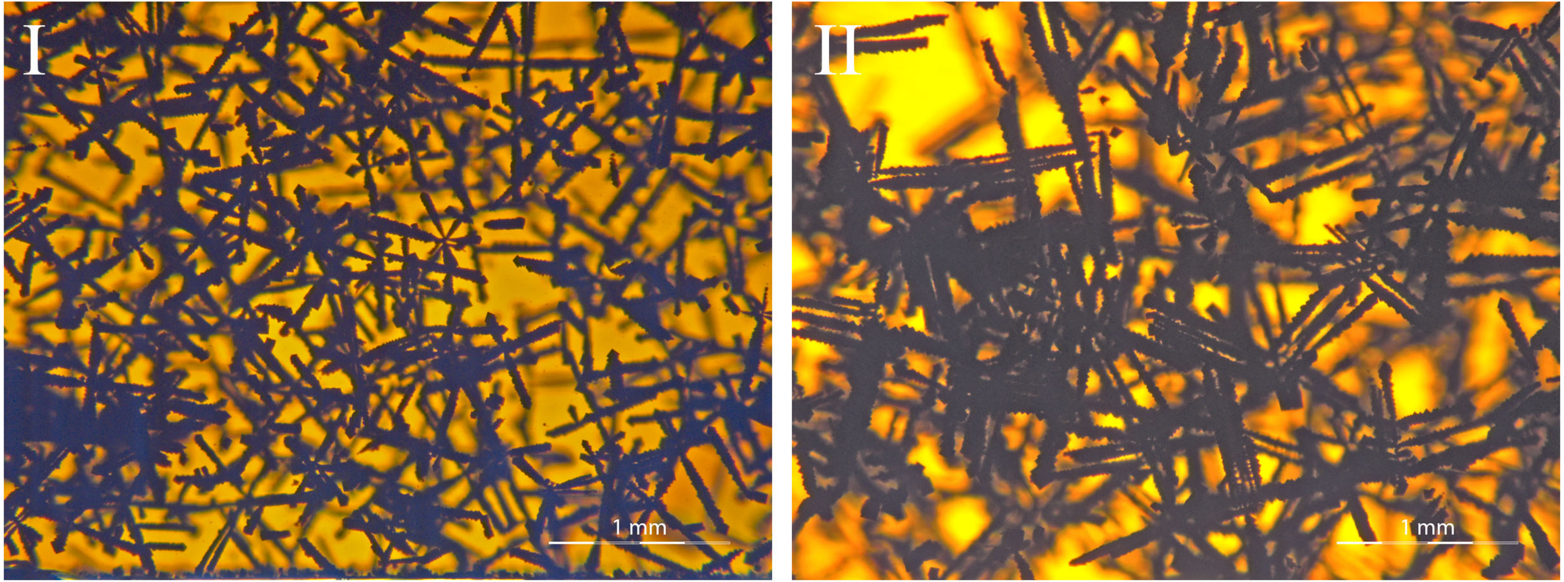
I
1 mm
II
1 mm

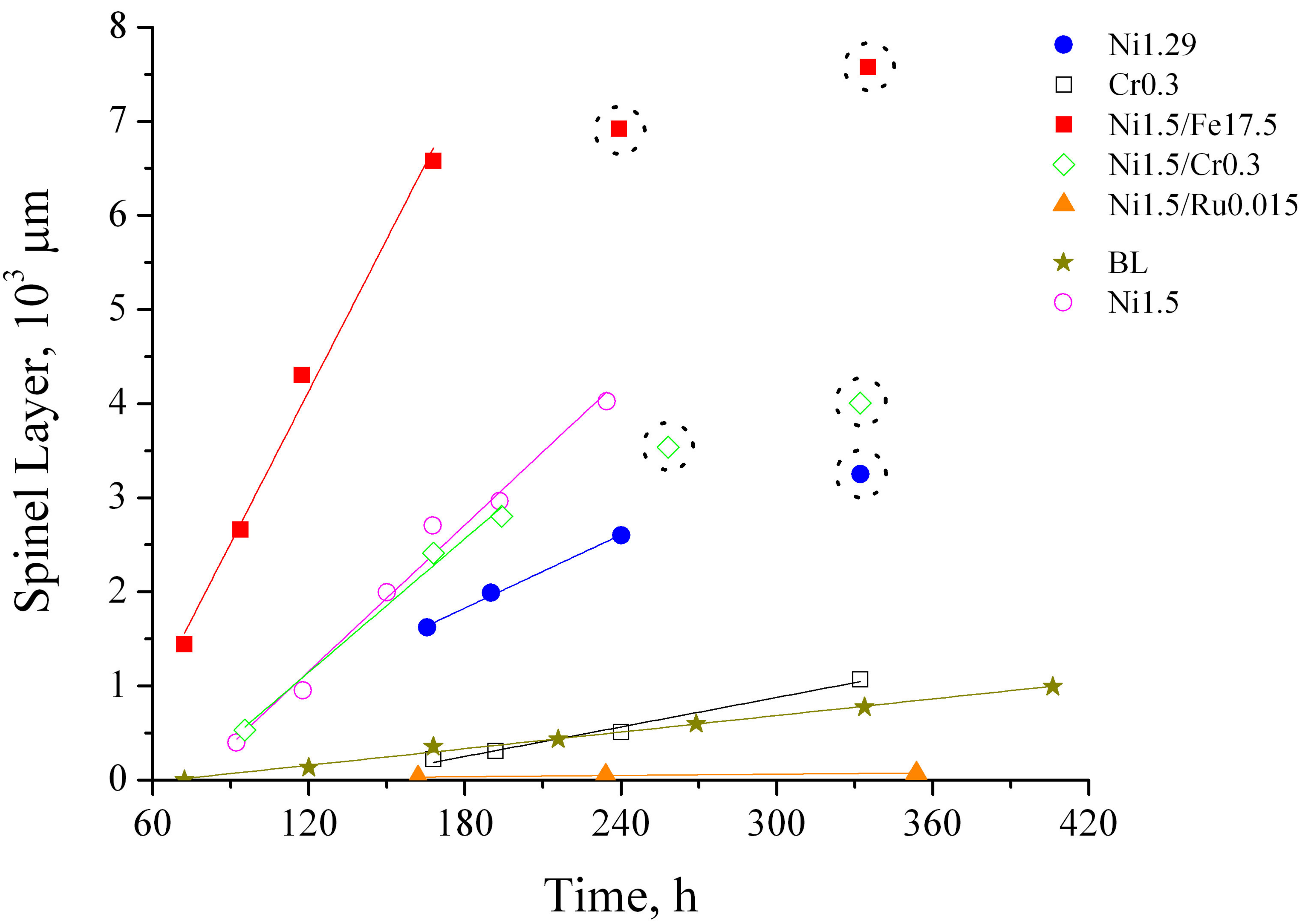
Spinel Layer, 10^3 µm
Time, h
0
1
2
3
4
5
6
7
8
60
120
180
240
300
360
420
Ni1.29
Cr0.3
Ni1.5/Fe17.5
Ni1.5/Cr0.3
Ni1.5/Ru0.015
BL
Ni1.5

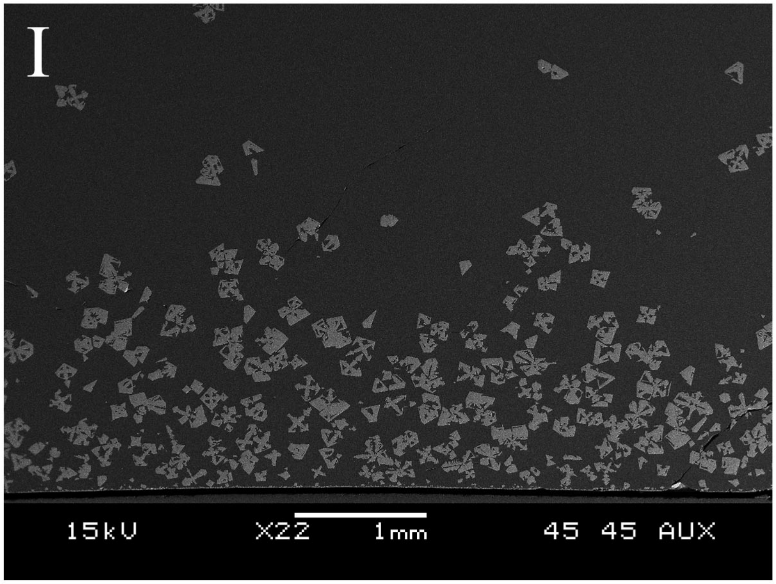
I
15kV
X22
1mm
45 45 AUX

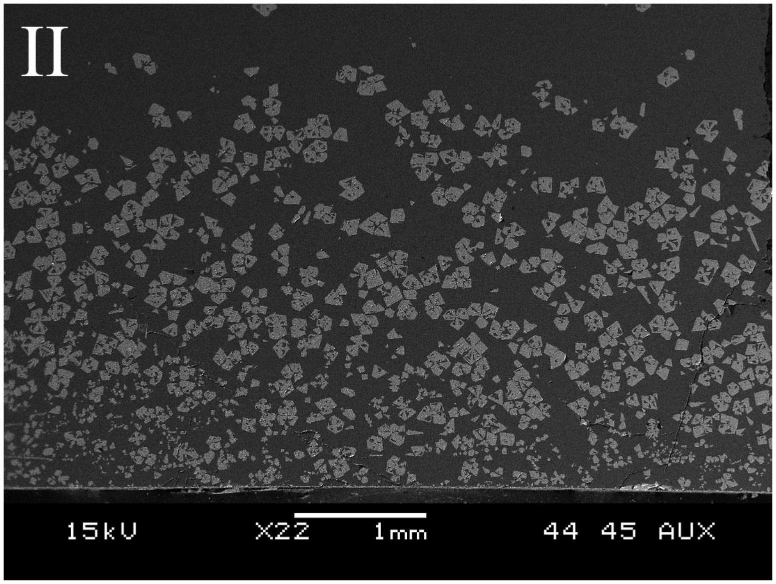
II
15kV
X22
1mm
44 45 AUX

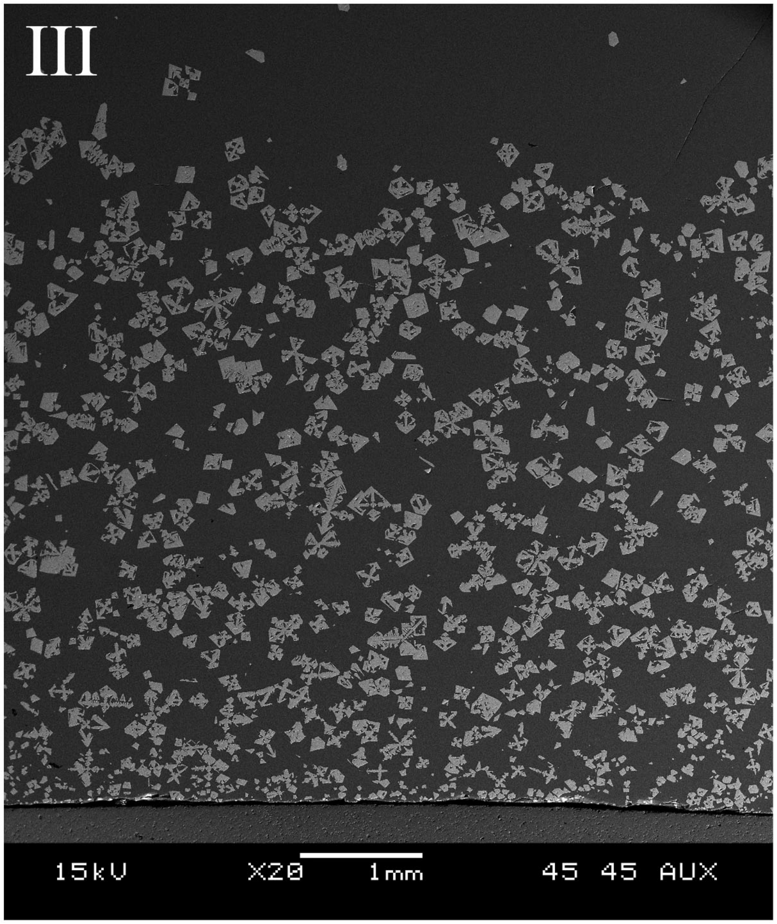
III
15kV
X20
1mm
45 45 AUX

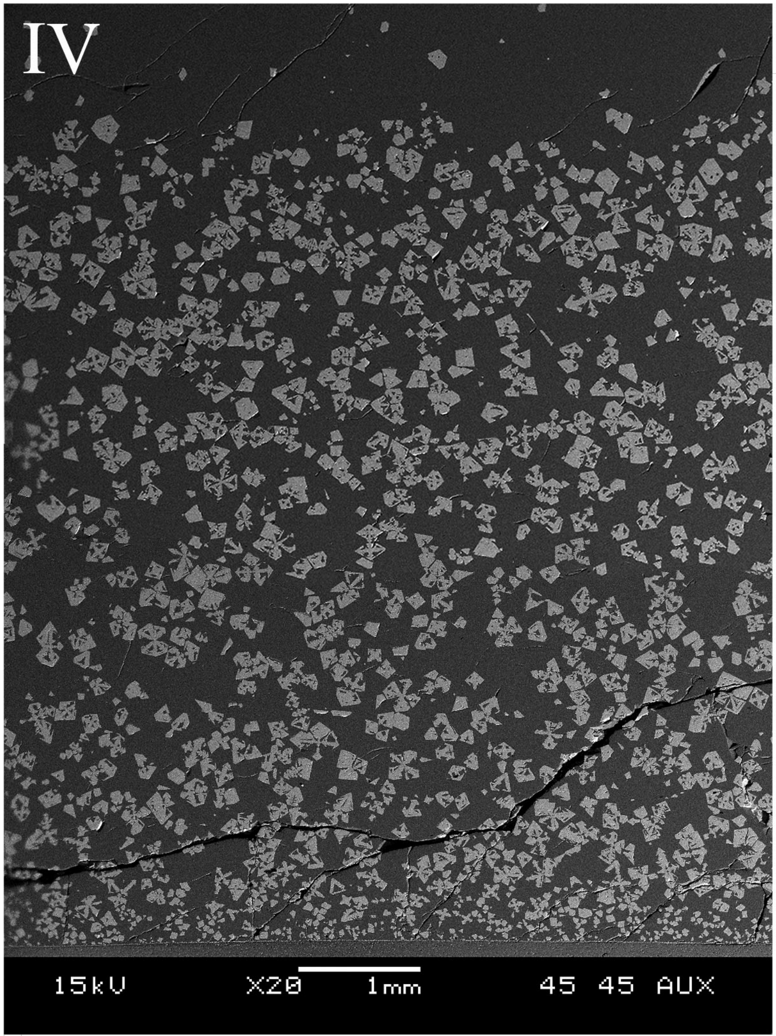
IV
15kV
X20
1mm
45 45 AUX

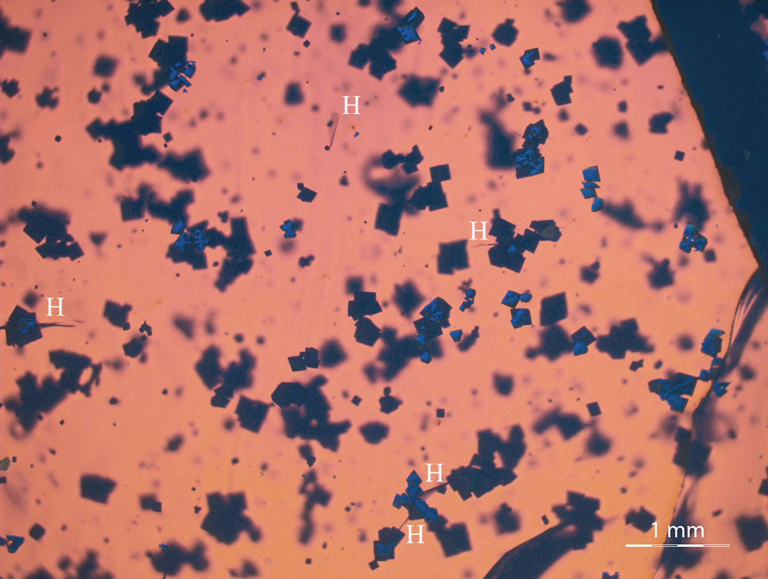
H
H
H
H
H
1 mm

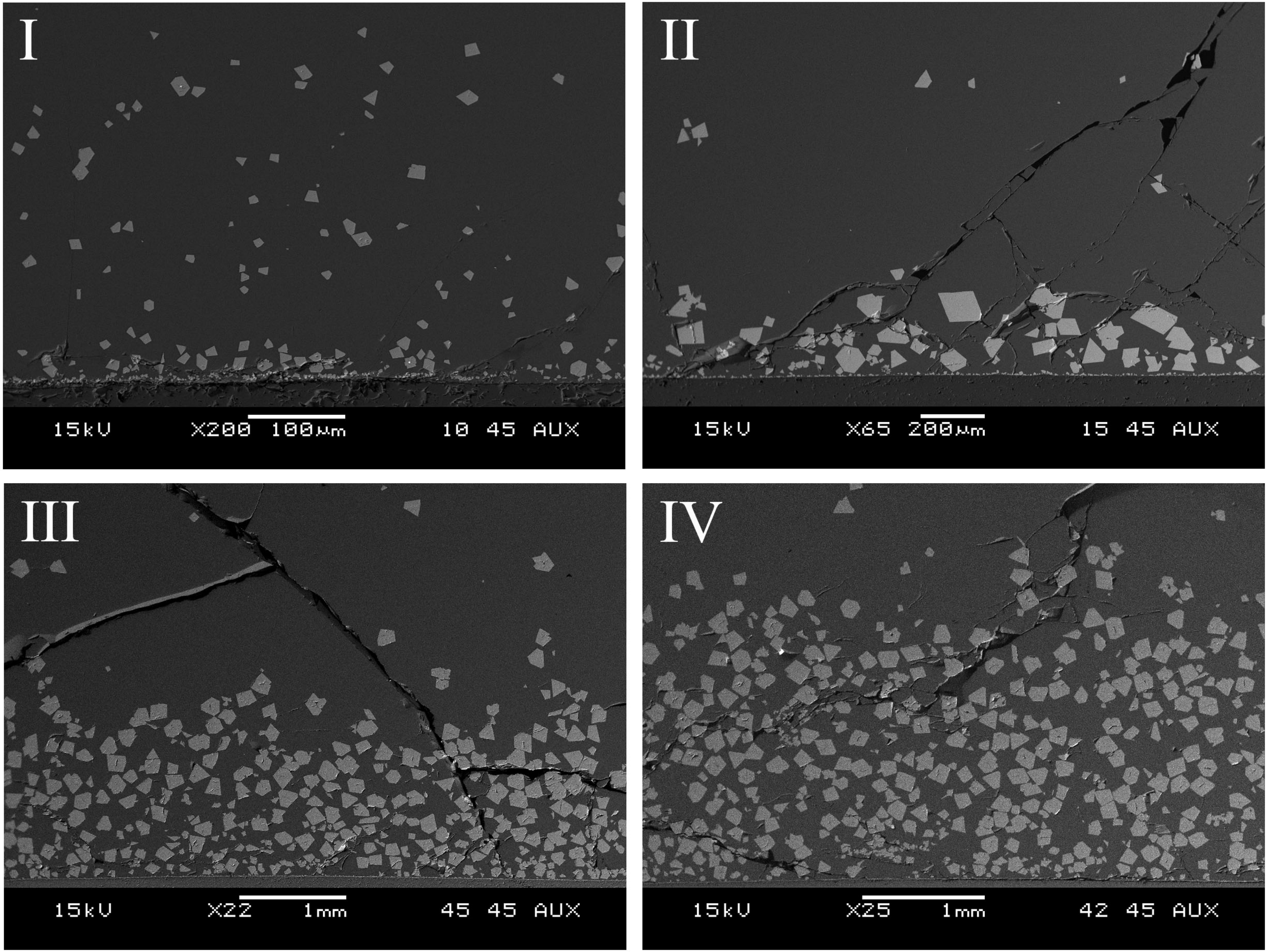
I
15kV X200 100µm 10 45 AUX
II
15kV X65 200µm 15 45 AUX
III
15kV X22 1mm 45 45 AUX
IV
15kV X25 1mm 42 45 AUX

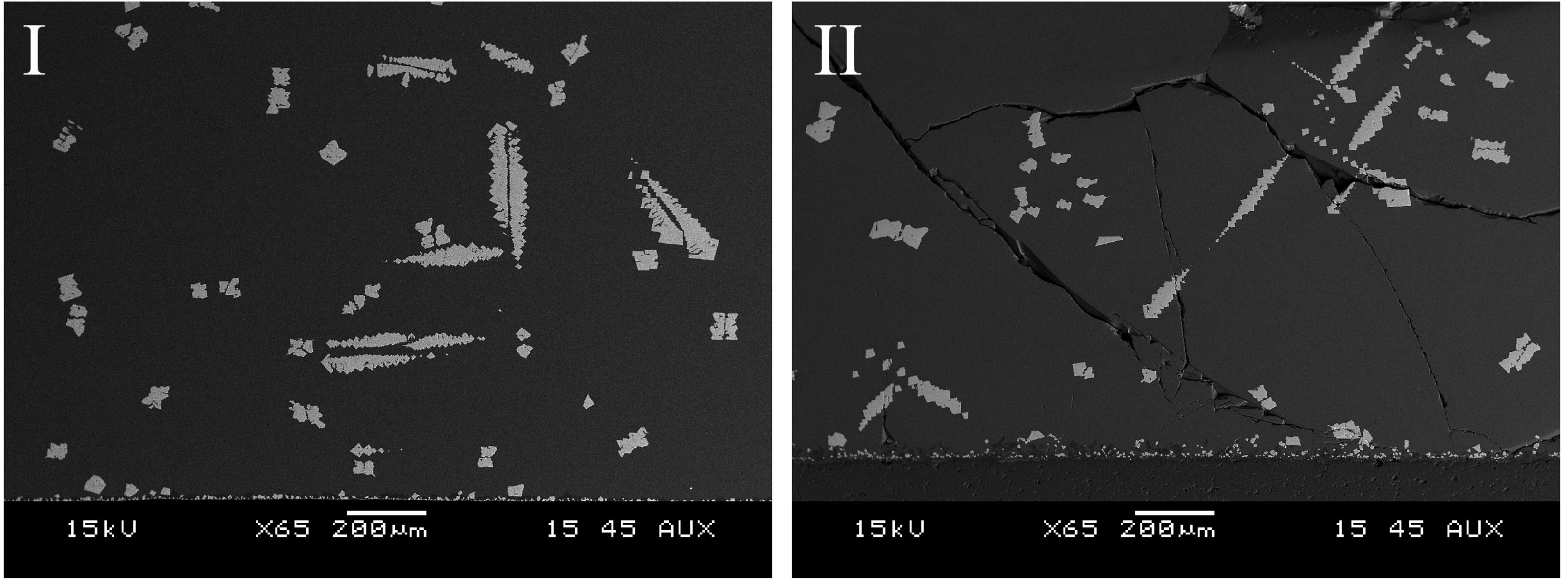
I
15kV
X65 200μm
15 45 AUX
II
15kV
X65 200μm
15 45 AUX

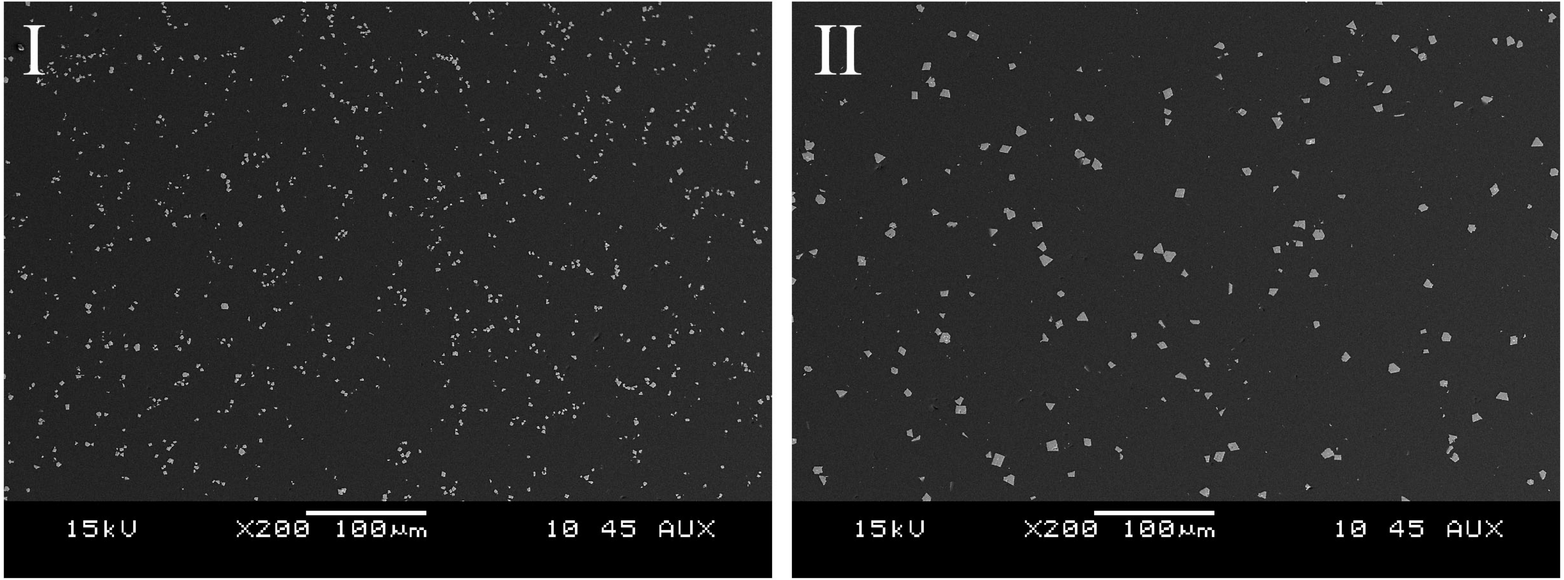
I
15kV X200 100µm 10 45 AUX
II
15kV X200 100µm 10 45 AUX

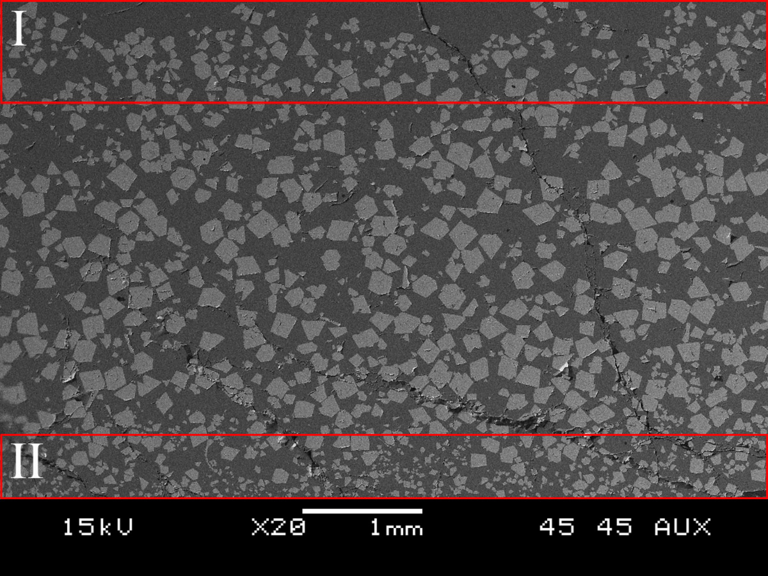
I
II
15kV
X20
1mm
45 45 AUX

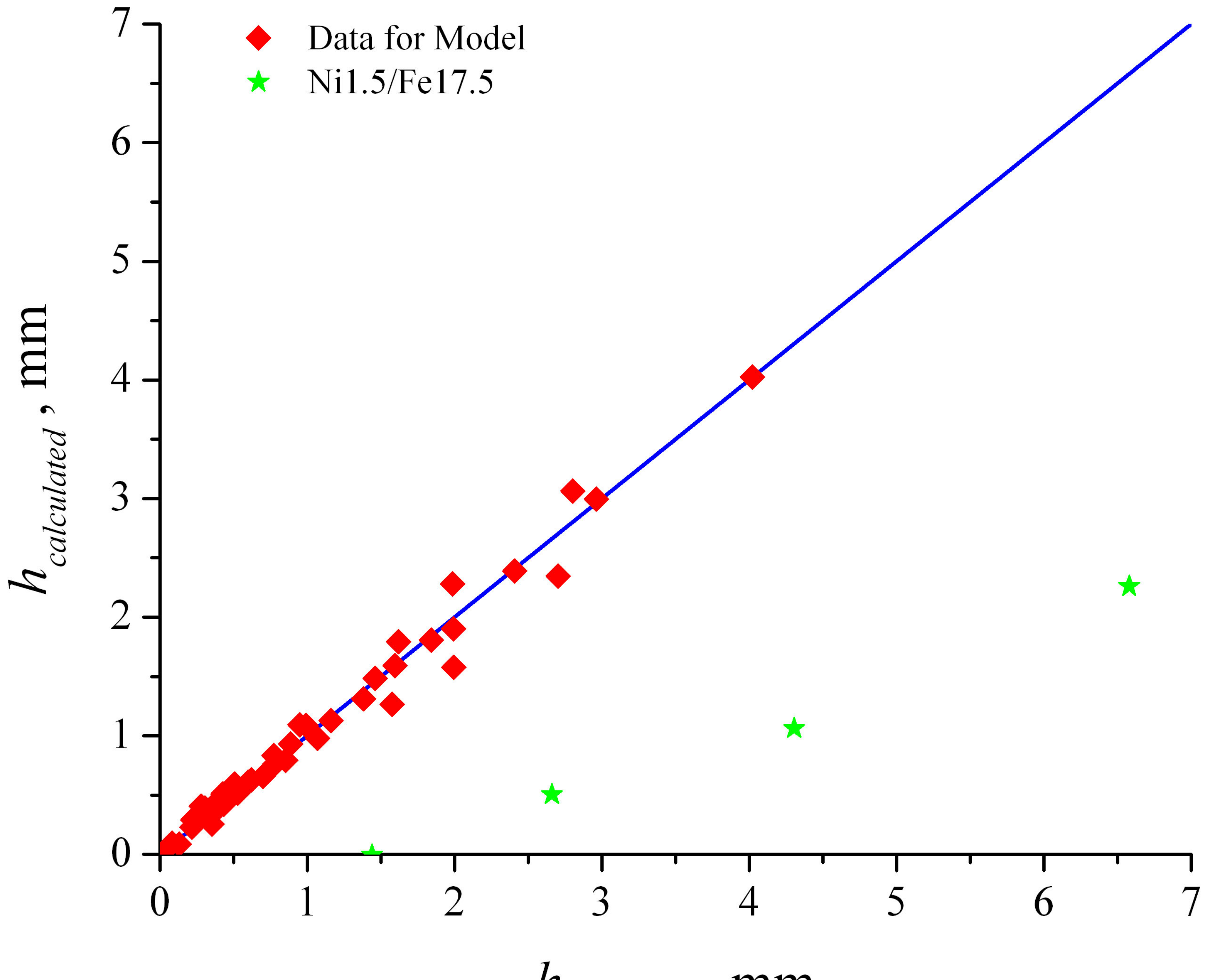
Data for Model
Ni1.5/Fe17.5
0
1
2
3
4
5
6
7
0
1
2
3
4
5
6
7
$h_{calculated}$, mm
$h_{measured}$, mm

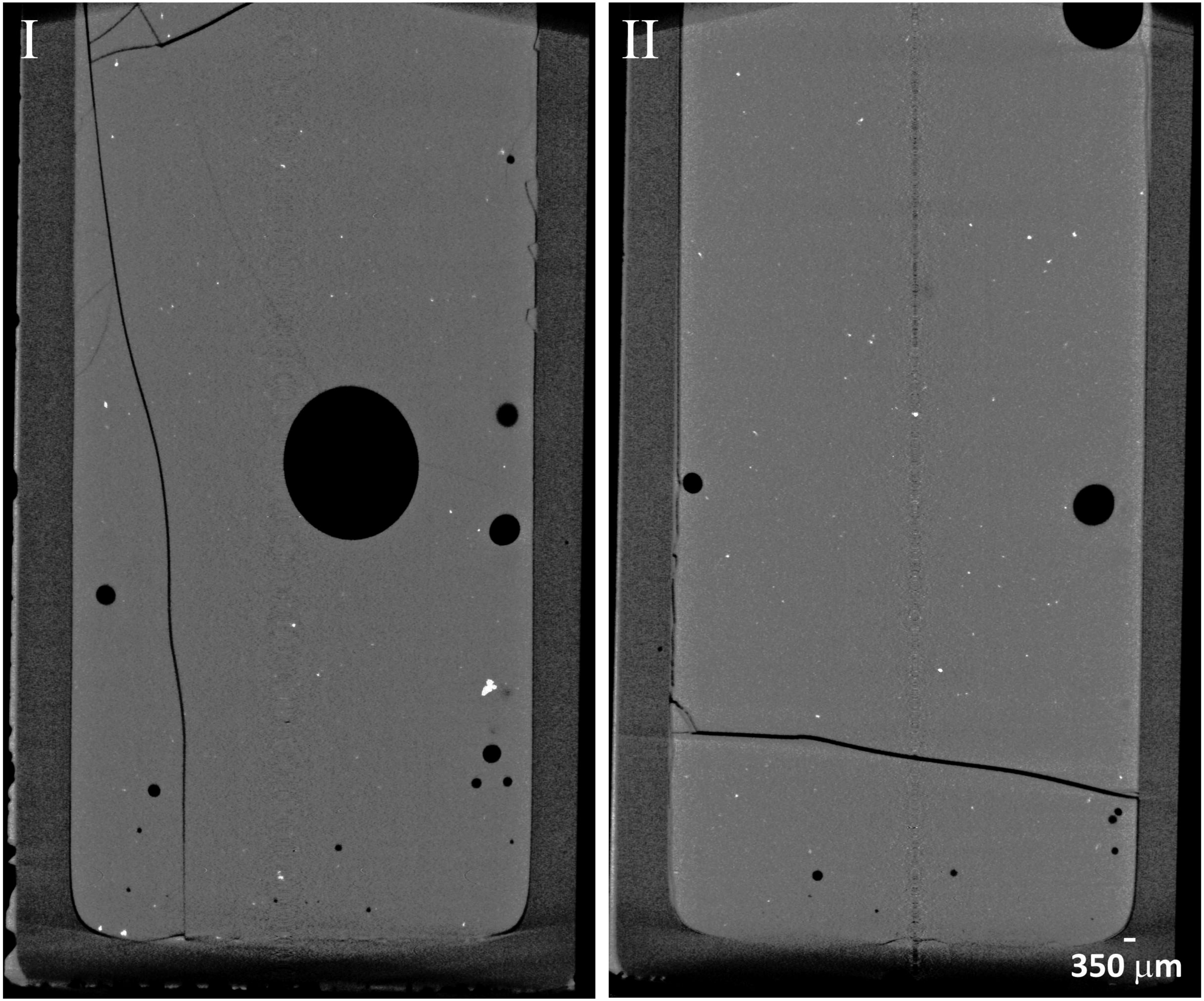
I
II
350 μm

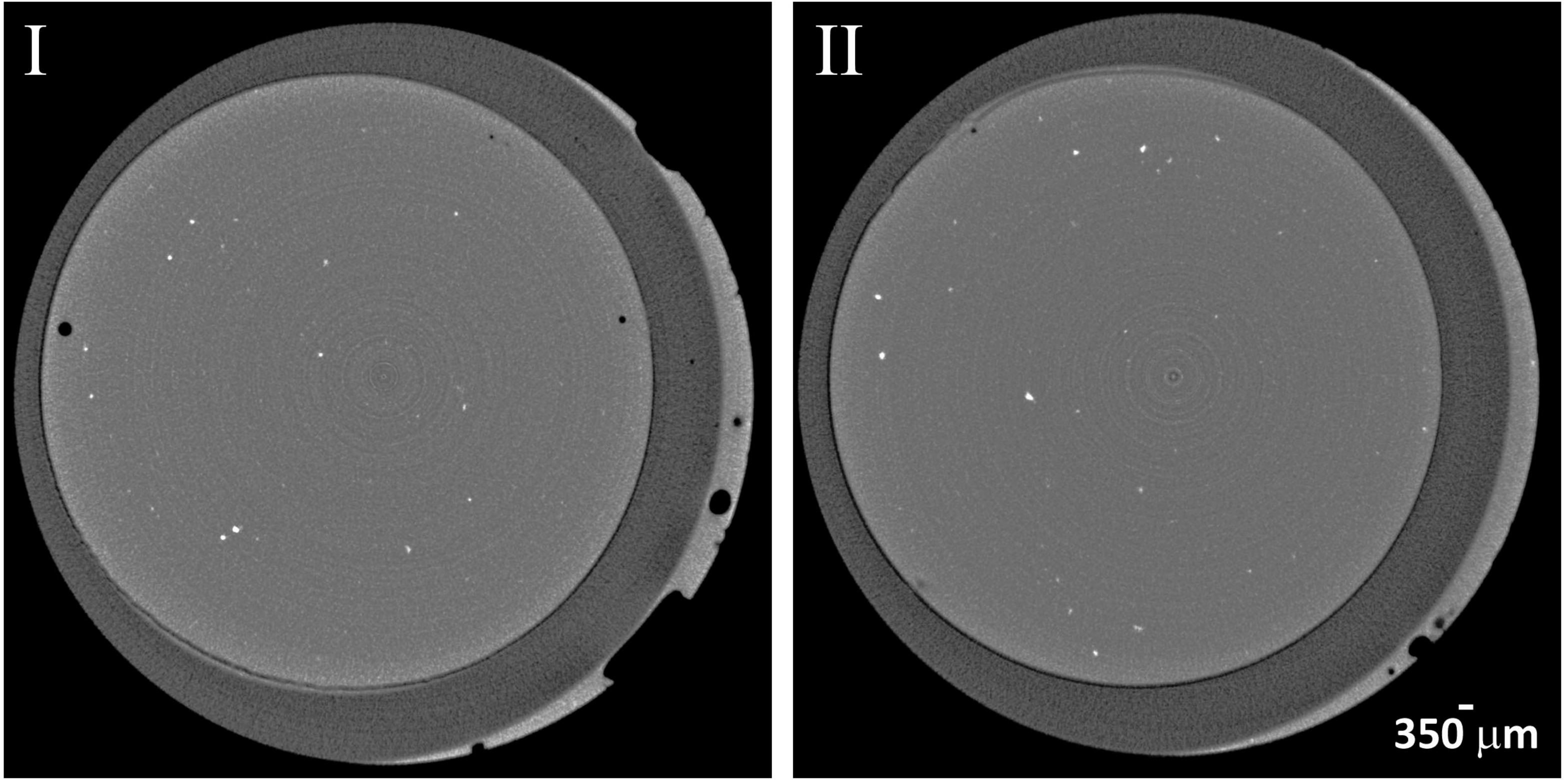
I
II
350 µm

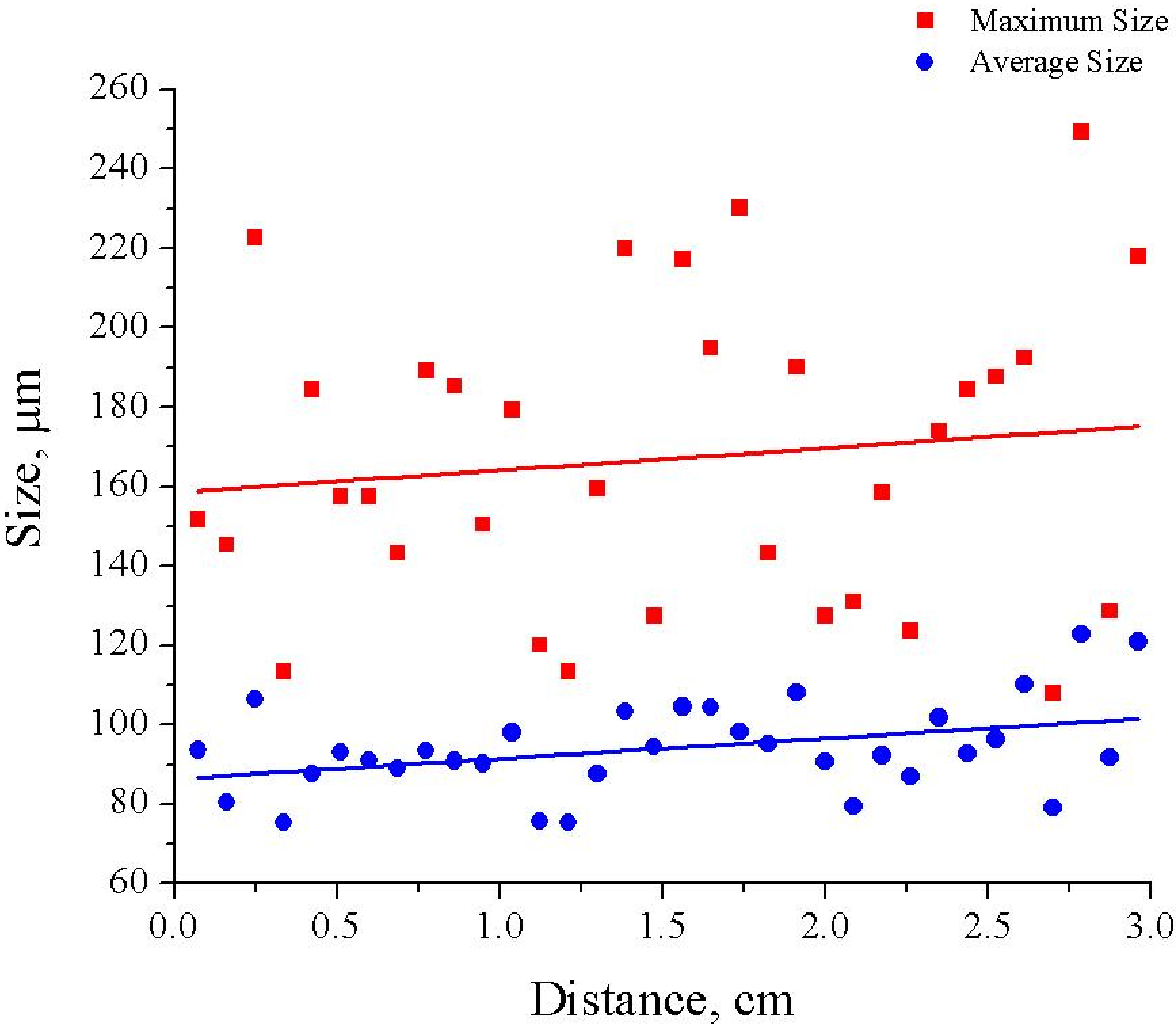

■ Maximum Size
● Average Size
260
240
220
200
180
160
140
120
100
80
60
Size, µm
0.0
0.5
1.0
1.5
2.0
2.5
3.0
Distance, cm

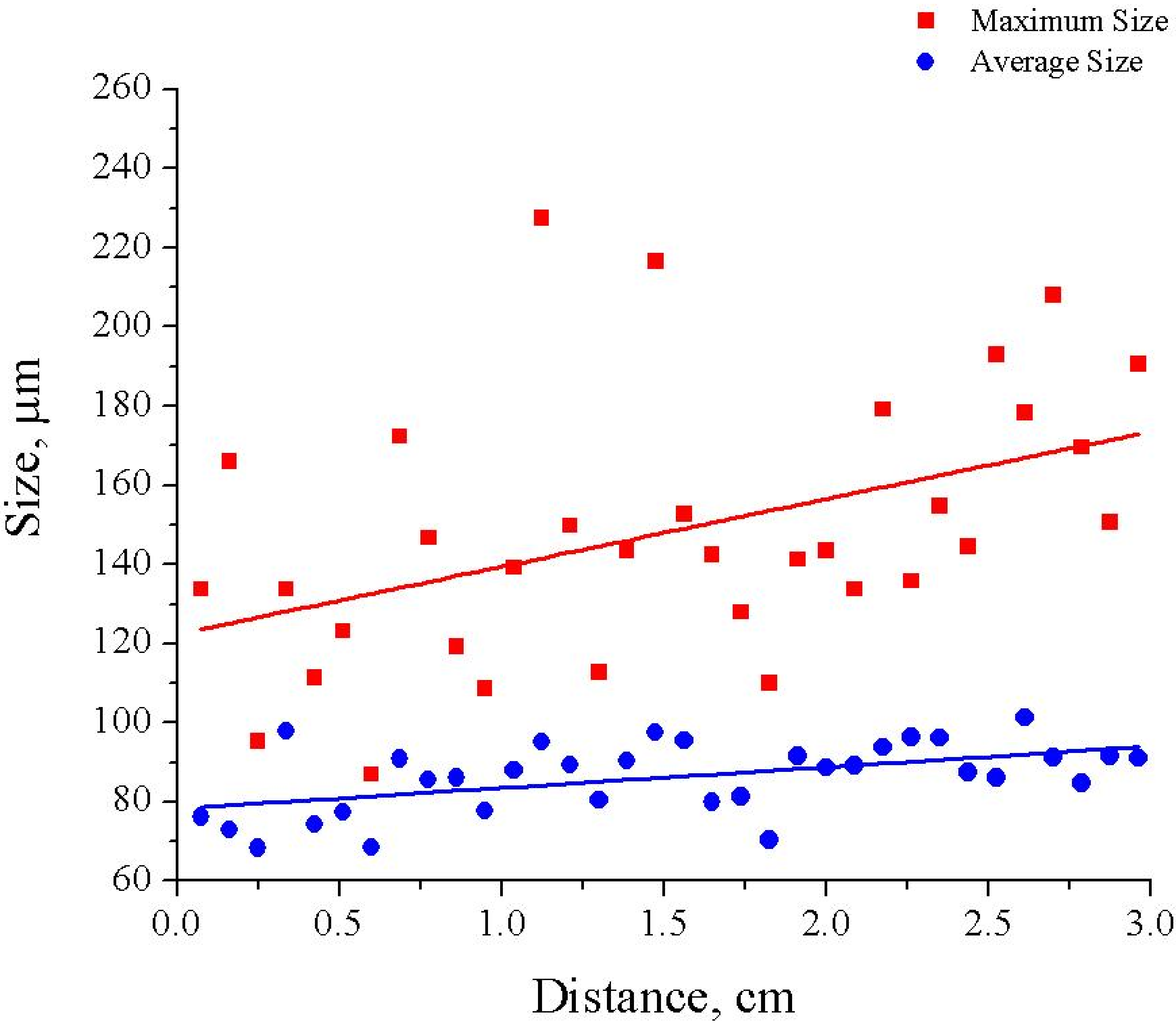
Maximum Size
Average Size
260
240
220
200
180
160
140
120
100
80
60
Size, µm
0.0
0.5
1.0
1.5
2.0
2.5
3.0
Distance, cm

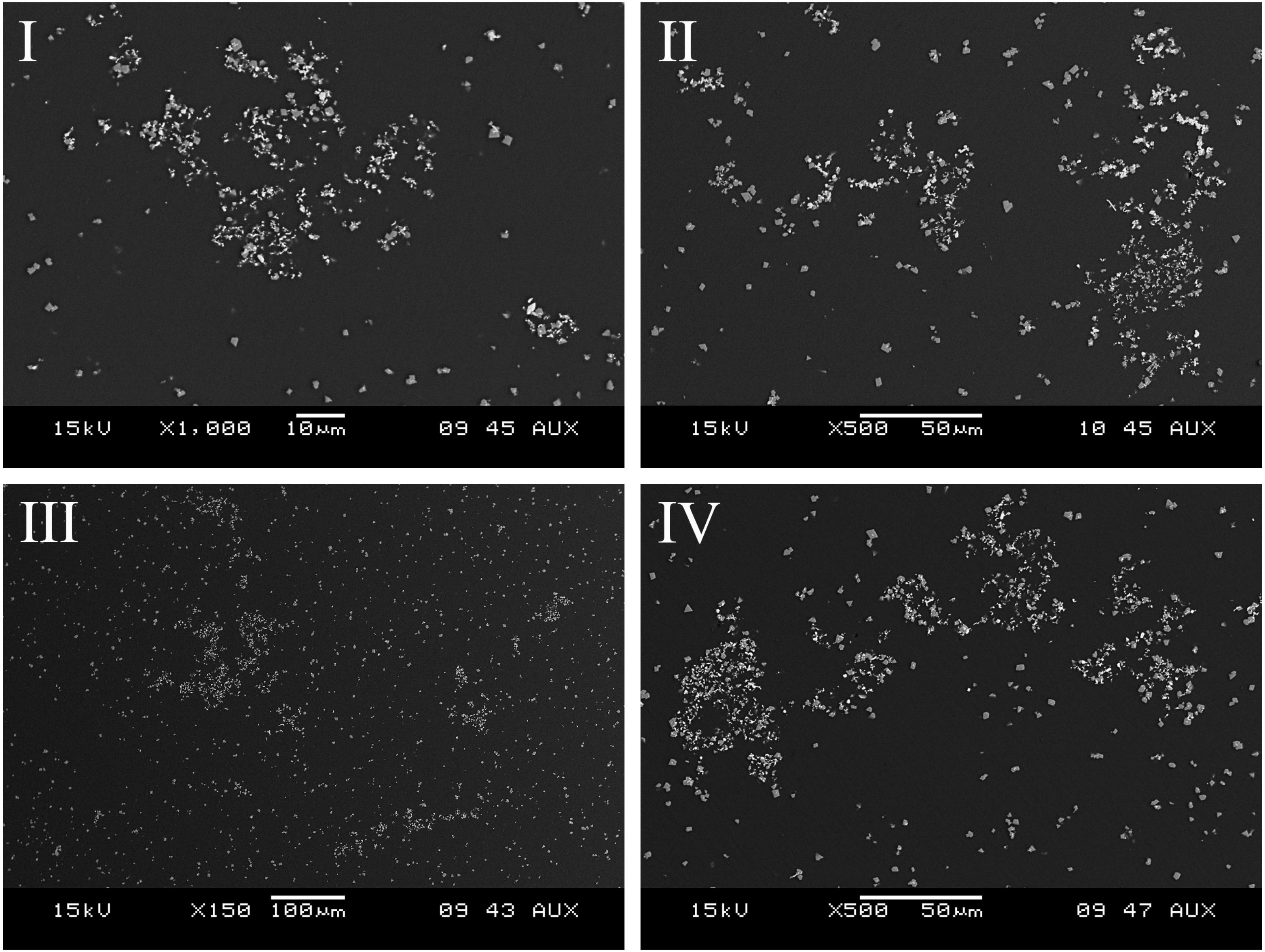
I
15kV X1,000 10µm 09 45 AUX
II
15kV X500 50µm 10 45 AUX
III
15kV X150 100µm 09 43 AUX
IV
15kV X500 50µm 09 47 AUX

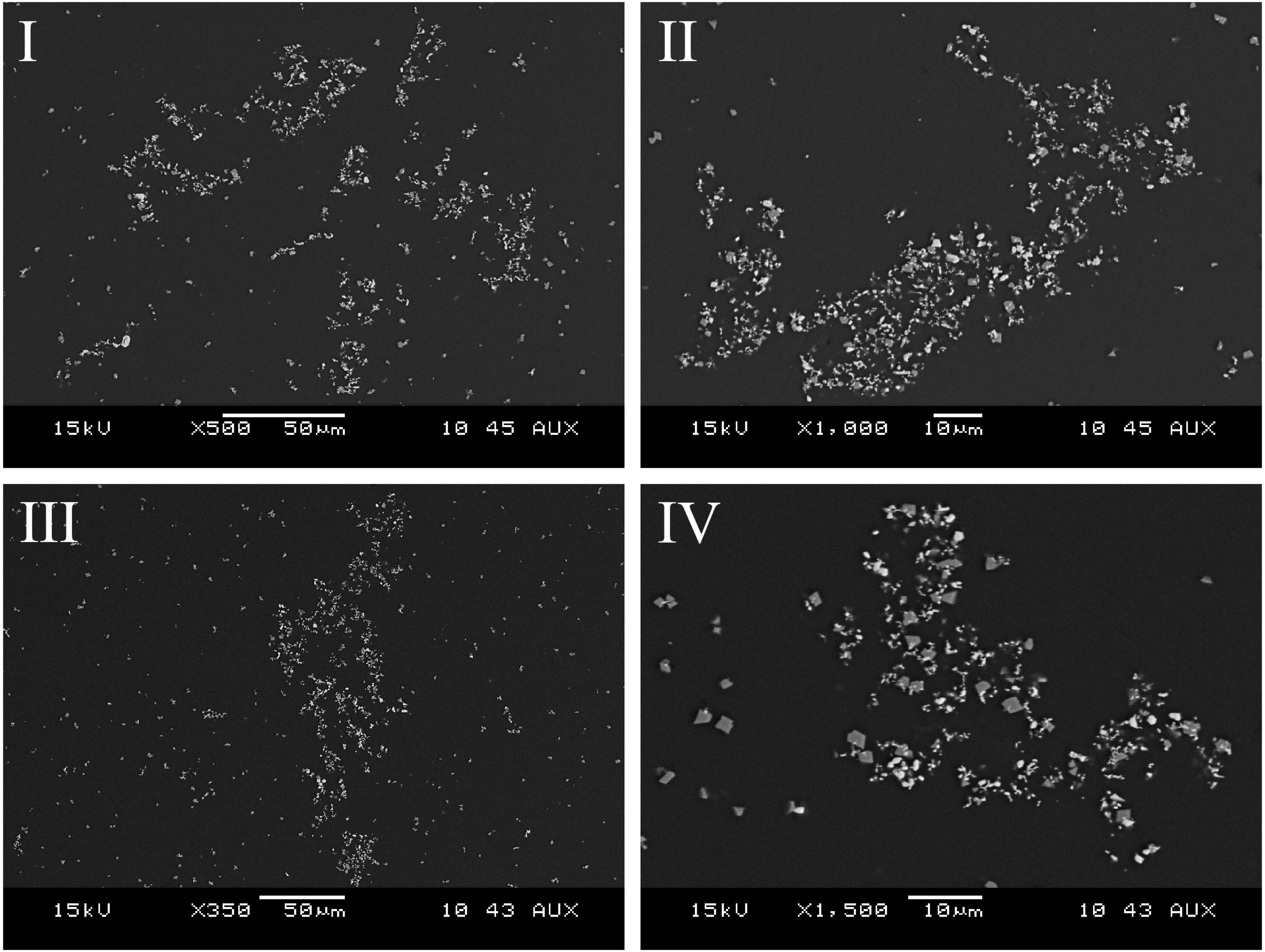
I
15kV X500 50μm 10 45 AUX
II
15kV X1,000 10μm 10 45 AUX
III
15kV X350 50μm 10 43 AUX
IV
15kV X1,500 10μm 10 43 AUX